Scientific Research Publishing

Open Journal of Geology, 2022, 12, 919-946
https://www.scirp.org/journal/ojg
ISSN Online: 2161-7589
ISSN Print: 2161-7570

Petrology and Geochemistry of Loukounga Metabasites Rocks: Constraining the Geodynamic Context of Neoproterozoic Nemba Complex in the Mayombe Belt

Ulrich Verne Matiaba Bazika[1,2*], Vicky Tendresse Télange Bouénitéla[1], Nelson Makamba Lekeba[1,2], Florent Boudzoumou[1,2]

[1]Laboratoire de géodynamique, Faculté des Sciences et Techniques, Université Marien Ngouabi, Brazzaville, Congo
[2]Département des Géosciences, Institut National de Recherches en Sciences Exacts et Naturelles, Brazzaville, Congo
Email: *iletbazika@gmail.com, Vicky_bouenitela@yahoo.fr, nelsonlekebamakamba@gmail.com, boudzoumouf@gmail.com

How to cite this paper: Bazika, U.V.M., Bouénitéla, V.T.T., Lekeba, N.M. and Boudzoumou, F. (2022) Petrology and Geochemistry of Loukounga Metabasites Rocks: Constraining the Geodynamic Context of Neoproterozoic Nemba Complex in the Mayombe Belt. *Open Journal of Geology*, **12**, 919-946.
https://doi.org/10.4236/ojg.2022.1211044

Received: October 6, 2022
Accepted: November 5, 2022
Published: November 16, 2022

Abstract

This study focuses on the metabasite rocks of the Nemba Complex of the Mayombe belt, an African segment of Araçuaï-West Congo Orogen (A-WCO) extending from the southwest of Gabon to the northwest of Angola. These metabasite rocks outcrops are in southwestern Congo along the Loukounga river. The Nemba complex is of Neoproterozoic age and represents the lower part of the west congolian Supergroup. The objective of this study is to constrain the geodynamic context of the Nemba complex from the petrology and geochemistry of the metabasites sampled in the Loukounga River. The observed rocks are composed of amphibolites, metagabbros, epidotites and greenschists and are affected by folding accompanied by flux schistosity and crenulation schistosity. Geochemical analyzes show that the rocks have a basic to ultrabasic chemical composition with SiO_2 contents between 41.85% and 58.23%. The geochemical composition of the major and traces elements shows that the rocks are basalts, basaltic andesites and andesites. The magma shows enrichment in LREE, LILE and depletion in HREE and HFSE. The multielement spectra show negative anomalies in Nb-Ta, Ti and a relatively low Nb/La ratio which characterize a lithospheric source contaminated by continental crust. Traces elements discrimination plots show that Loukounga metabasites are emplaced in intraplate geodynamic context like that associated with the basalts of the trap-types continental shelves and are possibly derived from mantle plumes contemporaneous with or slightly prior to magmatism.

Keywords

Nemba Complex, Mayombe, Loukounga, Greenstone, Geodynamic Context, Mantle Plumes

1. Introduction

The Mayombe belt is the African segment of the Araçuaï-West Congo Orogen (A-WCO) known from eastern Brazil to the west central Africa Atlantic margin. It extends from the southwest of Gabon to the northwest of Angola at around 1400 km of long and at around 100 to 150 km large [1]-[9] (**Figure 1**). The

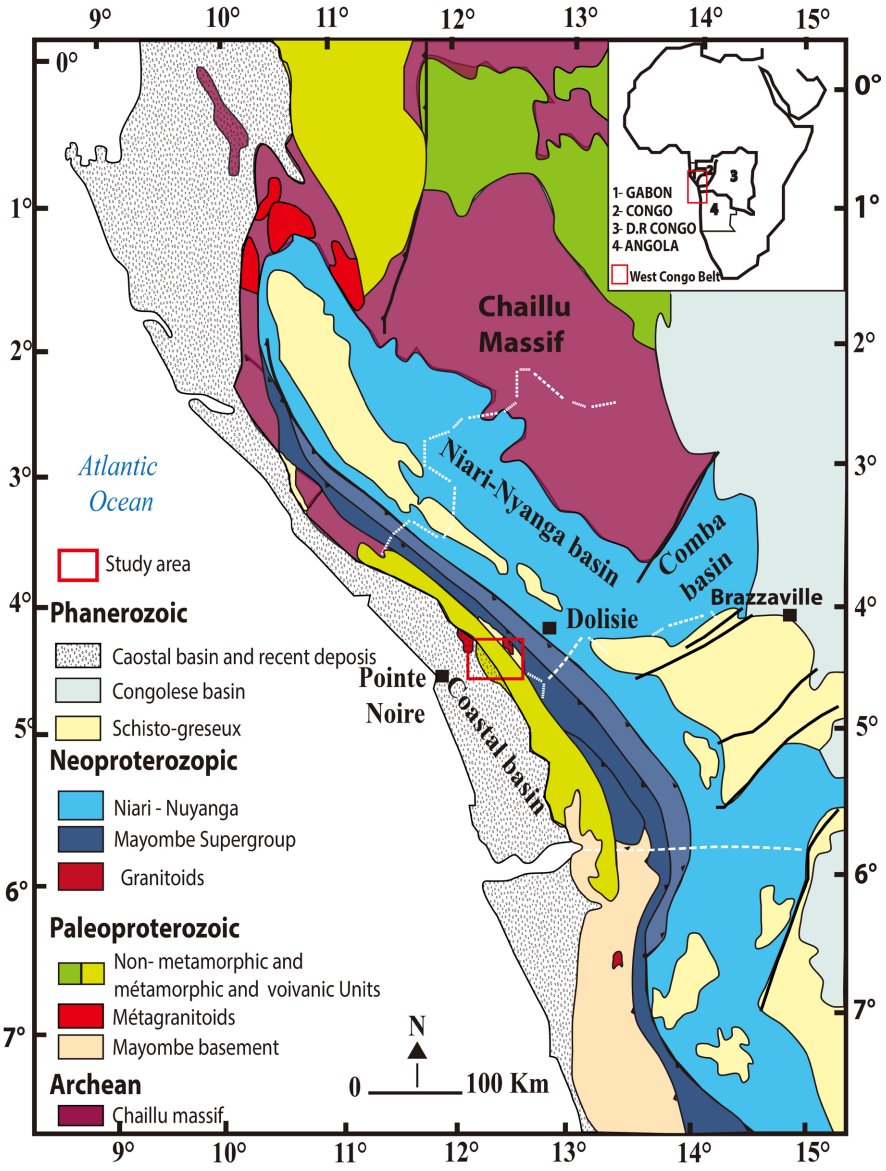

Figure 1. Geological map of archean to phanerozoic formations in the western part of central Africa (modified after [5] [6] and [8] by [12].

Mayombe belt is composed of assemblage of two or three tectono-metamorphism domains from west to east: the internal, intermediate and external domains [4] [5] [6] [7] [8] [10] [11] [12] in which appear progressively the older to younger formations.

The internal domain is formed by paleoproterozoic units composed of gneiss, quartzites, meta-sandstone, schist, metabasites and meta-volcanites rocks [5] [8] [11] [13]. The intermediate and external domains are made of the neoproterozoic west congolian Supergroup. The intermediate domain is constituted by the lower part of the west congolian Supergroup and contains siliciclastic, volcanoclastic and metabasite basic rocks. These metabasites represent a large formation called Nemba Complex. The external domain is composed of the deformed upper part of the west congolian Supergroup made of siliciclastic, physico-chemical and glacial neoproterozoic formation. These formations take also part in the Niari-Nyanga foreland basin where they become on subtabular position on the Chaillu craton, a fragment of the large Congo craton.

This study is focused on the metabasite rocks (or greenstones) outcropping in Loukounga river in the southwestern part of the Mayombe belt which can be attached to Nemba Complex whose geodynamic context is controversial. Greenstones are important landmarks in Precambrian blocks and are integral to continental rifting and collision zones. It is one of the important indicators of crustal stabilization events, assembly and dispersal of supercontinents. They are also thought to be valuable time markers, as they record the rate of intraplate mantle melting events over time. The metabasites (or greenstones) of Nemba Complex are considered as an intraplate volcanic coeval of rifting and fragmentation of Rodinia supercontinent [6] [11] [14] and deformed during panafrican event or as an oceanic crust involved in collisional kibarian event [15]. The metabasites rocks of Loukounga River can be attached to the Nemba Complex outcrops near the paleoproterozoic gneiss and micaschists of Loukoula Group in Congo. Thus, the study of these metabasites (or greenstone) of Loukounga aims to characterize the petrogenesis and the geodynamic context and to contribute to scientific knowledge of Nemba complex.

2. Geological Setting

The studied rocks are situated in the median part of the Mayombe belt and outcrops in the Loukounga River situated in Mbéna locality of Congo Republic (**Figure 2**).

2.1. Lithostratigraphy of the West Congolian Supergroup of the Mayombe Belt

The internal domain is composed by three distinct palaeoproterozoic units [8] [11] (**Figure 3**): 1) the Loémé Unit outcropping in the southern part of the belt. It is composed of schists, ortho and para gneiss intruded by the Bilinga and Bilala metagranitoids whose ages U-Pb on zircon, ID-TIMS are respectively 2048 ±

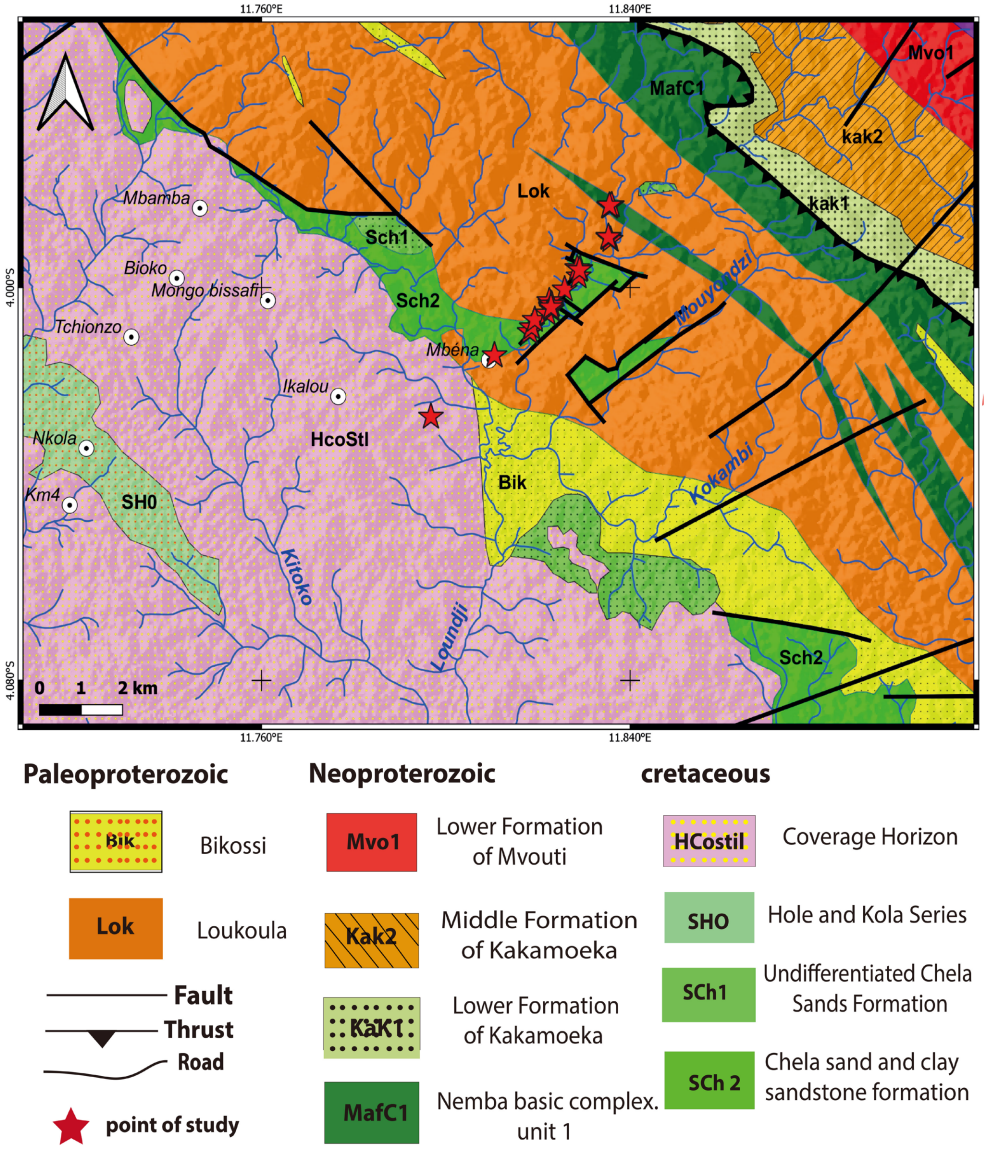

Figure 2. Extract of the portion of the Mayombe belt and coastal basin formations showing Loukounga point studied and Mbéna area on the geological map of [3].

12 Ma and 2014 ± 56 Ma [8] [16] and U/Pb on zircon, SIMS age is 2028 ± 12 Ma [11]; 2) the Loukoula Unit outcropping in the northern part of the belt contains para and orthogneiss, micaschists, schists, amphibolites and quartzites cut locally by Les Saras granodiorite plutons and dolerite dykes. Les Saras granodiorite yielded U/Pb zircon age of 1920 ± 10 Ma, TE-TIMS [17] and 2000 ± 80 Ma, ID-TIMS [5], and 2038 ± 10 Ma, SIMS [11]; 3) the Bikossi Unit is composed essentially by quartzite and contains locally conglomeratic level, micaschists, schists and amphibolites [3] [4] [8] [10] [11] [15].

Detrital zircon geochronology in the quartzite yielded age of sources between 2.20 Ga to 2.00 Ga [8] and 3.08 Ga to 2.04 Ga [11]. This unit is cut by Mont Kanda and Mfoubou granites which yield respectively ages of 928 to 932, U-Pb zircon, LA-ICP-MS [11] and 1050 ± 25 Ma, U-Pb zircon, ID-TIMS [16].

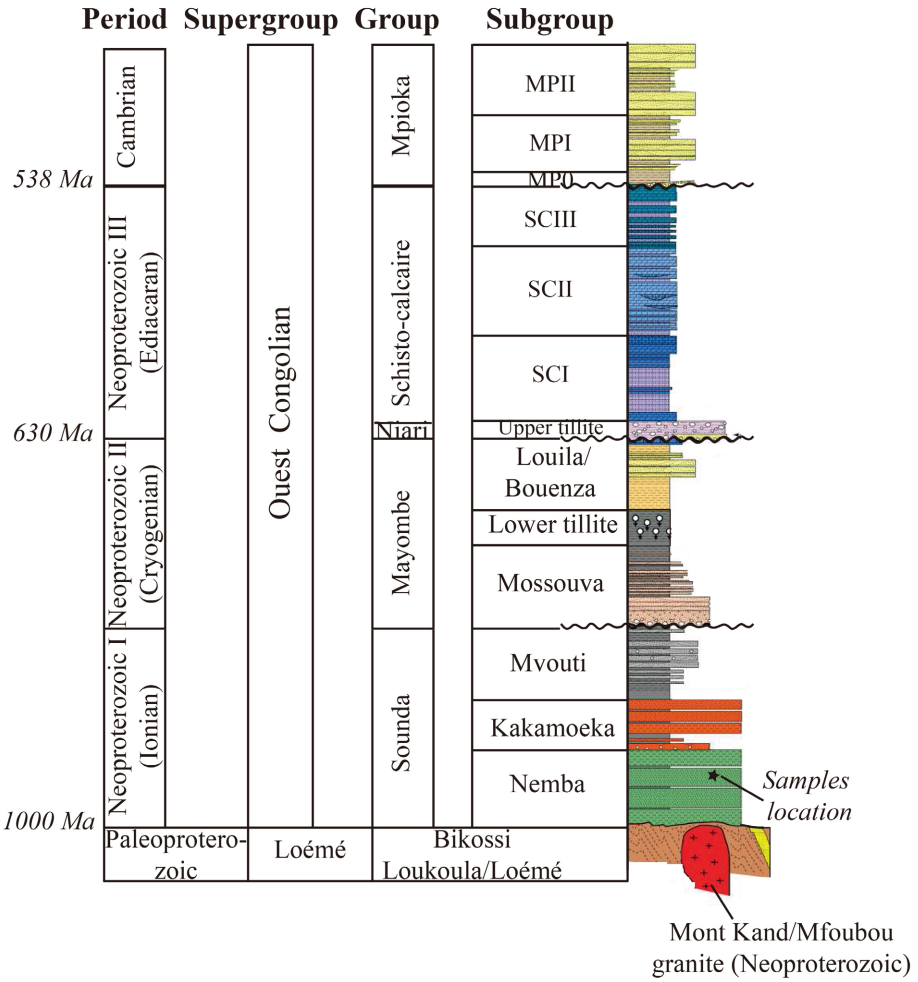

Figure 3. Simplified lithostratigraphy of the west congolian Supergroup of the Mayombe belt from [11].

In the Araçuaï belt in Brazil, the internal domain is represented by the paleo-mesoproterozoic Espinhaço Supergroup composed of vulcanite, quartz-sandstone, conglomerate, pelite, and subordinate carbonate [18] [19] [20] deposited at around 1.75 Ga [21].

The intermediate domain is represented by the lower part of the west congolian Supergroup [6] [11] (**Figure 3**). It comprises: 1) the Sounda Group containing the Nemba Complex Subgroup composed of metagabbros, metabasalts, amphibolites and greenschists and dated at 915 ± 8 Ma, U-Pb zircon [11]. Similar basic magmatic rocks, the Gangila basic rocks of the Zadinian Group in RD Congo yielded age comprise between 999 ± 7 Ma and 920 ± 8 Ma. [6]. The metabasite rocks of the Nemba Complex are considered derived from tholeiitic lava flows containing pillow structures [15] or a continental tholeiitic rift magma [11] [14]; 2) the Kakamoeka Subgroup, or Mayumbian Group of RD Congo, composed of conglomerates, quartzites, graphitic schists, ignimbrites, rhyolites, tuffs, metabasic rocks and yielded age between 920 ± 8 Ma and 912 ± 7 Ma [6]; 3) the Mvouti Subgroup constituted of chlorito-schists, ampelitics schists, qua-

rtzites, meta-sandstones and meta-arkoses; 4) the Moussouva Subgroup composed of quartzites and schists. The lower part of west congolian Supergroup is considered as an aulacogen deposit [4] or a syn-rift sequences [11].

The external domain is represented by the upper west congolian Supergroup (**Figure 3**). It comprises the lower Diamictite (or Tillite) composed by glaciogenic [3] [4] [8] [22] or a mud flow deposits [2] [11] [23] constituted by black calcareous shale containing heterogeneous, heterometric and heteromorphic pebbles and boulders. An intercalation of basic magmatic rocks is described in RD Congo. It is underlaid by the Louila Subgroup composed of meta-sandstones, locally conglomeratic, quartzites, quartzo-schists and schists with intercalation of limestones and calcschists [3] [4] [8] [11] [22]. The Louila formation is overcome by the glacio-marine upper Diamictite formation [4] of marinoan age [24]. In the top, the Schisto-calcaire Group made of thick carbonated platform deposits [3] [23] [25] [26] [27] contains shales and siltstones intercalations and his folded outcrops area constituted the transitional zone with the subtabular deposits of the Niari-Nyanga basin. The upper west congolian Supergroup is considered as a passive margin deposit [11].

In Araçuaï orogen, neoproterozoic sediments is represented by the Macaubas Group whose age is situated between 1000 Ma and 850 Ma [28] [29]. The sediments took place in rift basin which evolved into an arrow ocean basin [30]. The Macaubas Group contains in the lower part a tillite (or diamictite), sandstones, pelites, and subordinate basic volcanics. It passes in the east and south of the belt to thick sequences of distal pelites with intercalations of sandy turbidites [29] [31] and an ophiolitic assemblage, composed of basalt, chert, banded-iron formation, gabbro, plagiogranite, and ultramafics rocks. Mafic rocks of the assemblage yield a Sm-Nd isochron age of 816 ± 72 Ma (with εNd = +3.8), interpreted as the time of magmatic crystallization [32].

2.2. Deformation and Metamorphism

The deformation and the metamorphism in the Mayombe belt decrease from the internal domain to the external domain. They whole domains are affected by thrust faults with northeast vergence.

In the intermediate and external domains two deformations phases oriented roughly NW-SE are observed. The first phase in the west of the intermediate domain is marked by isoclinal folds with an eastern vergence and penetrative cleavage schistosity (S_1) and become right folds in the external domain. The second phase is characterized by right fold slightly verged bearing a strong crenulation schistosity (S_2) in the intermediate domain. This crenulation schistosity (S_2) becomes discrete in the external domain. These two phases of deformation are attributed to panafrican events [4] [5] [8] [10] [11] [33].

The metamorphism is amphibolite facies in internal domain [10] [11] [12] and decrease to greenschists facies in the intermediate domain and passes to anchizone facies in the external domain at the limit of the Niari-Nyanga basin

[11].

In the internal domain, the palaeoproterozoic basement is affected by strong crenulation schistosity (S_2) oriented NW-SE which refolds paragneissic foliation [4] [8] [10] [11] [12] [33]. Locally crenulation schistosity (S_3) oriented NE-SW is described in Loeme unit [4]. The foliation of paleoproterozoic formation is attributed to eburnean event [4] [10] [11] [12] and the crenulation schistosity (S_2) is from panafrican event [4] [12].

3. Material and Method

3.1. Sampling

The samples are collected at the western part of the Mayombe belt (**Figure 2**) in the Loukounga River near the Mbéna area. This zone is characterized by the passage of paleoproterozoic unit to neoproterozoic formations. Basics samples collected are attributed to Neoproterozoic Nemba Complex. Fine sections of selected samples for petrological determination are confectioned in laboratory of the fine sections of University of Rennes 2, France.

3.2. Analytical Method

Geochemical analyses of major, trace and rare earth elements were done to evaluate the petrogenesis of rocks. Major, trace and rare earth elements were determined on selection samples without sign of weathering and/or a slight hydrothermal overprint. Samples are powdered and placed in fusion with $LiBO_2$ and dilute by HNO_3 and performed by inductively coupled plasma-mass spectrometry (ICP-MS) and inductively coupled plasma atomic emission spectrometry (ICP-OES) in the "Centre de Recherches Pétrographique et Géochimique" (CRPG) of Nancy, France. The quality control is realized with international geostandards.

4. Results

4.1. Macroscopic Description

The rock outcrops along the Loukounga river and are made of paragneiss, micaschists amphibolites, metagabbros, and greenschists (**Figure 4**).

Paragneiss (**Figure 4(a)**) are composed of an alternating millimetric to centimetric rich biotite levels and rich quartzo-feldspathic levels. They are attributed to paleoproterozoic unit which constituted the basement of the Mayombe belt. Amphibolites (**Figure 4(a)**) are found locally in contact with paleoproterozoic paragneiss of Loukoula unit. In some places they are massive but are generally strongly deformed with cleavage schistosity (S_1) and discrete crenulation schistosity (S_2) and shows right fold accompanied of thrusting movement (**Figure 4(b)**). Metagabbros (**Figure 4(c)**) are in massive lenticular corps surrounded by fine matrix made of greenschist. Micaschists (**Figure 4(d)**) are in alternation with chloritoschists and bear crenulation schistosity. The whole rocks are locally affected by quartz and calcite veins that run parallel to the schistosity.

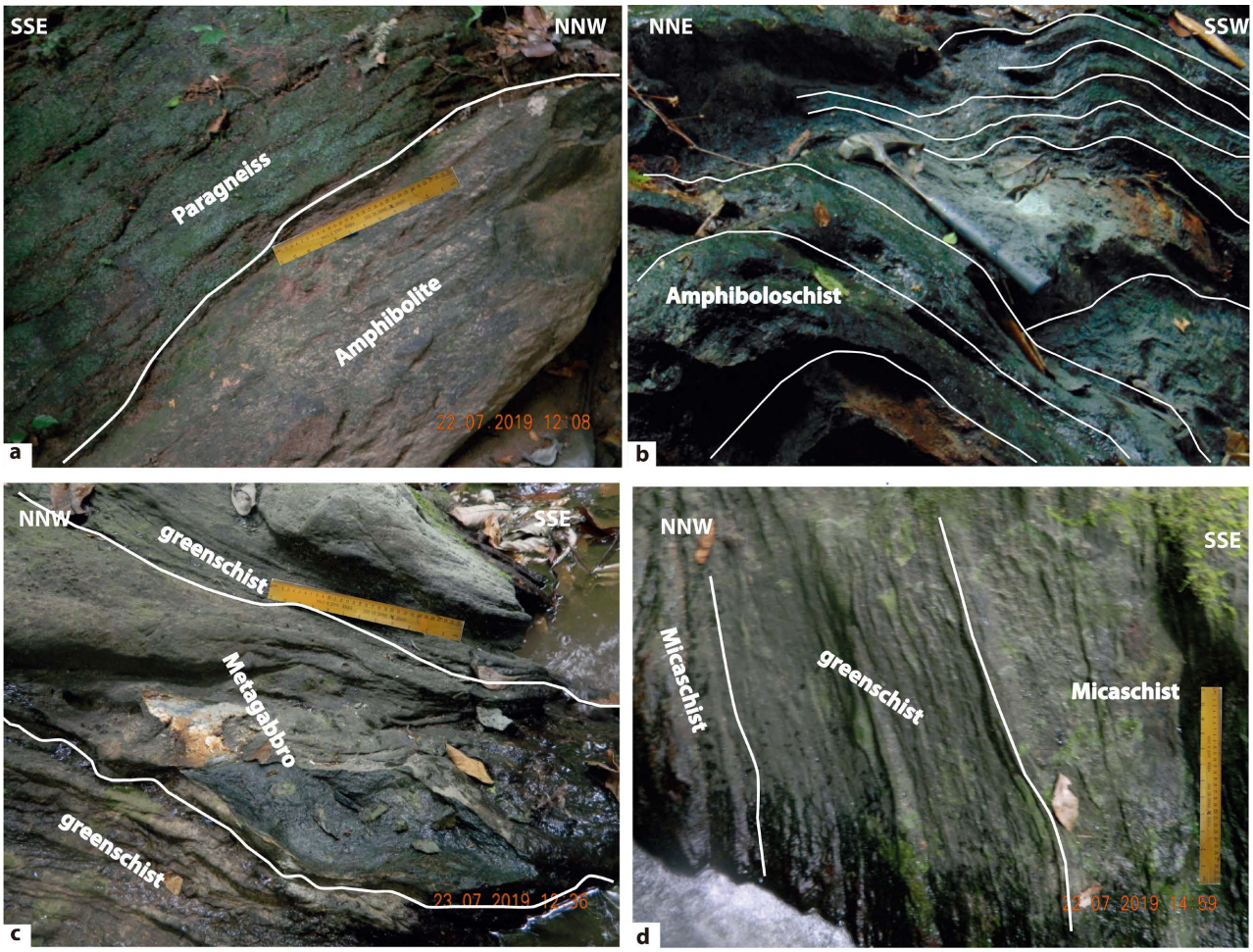

Figure 4. Outcrops of paragneiss of Loukoula Unit and metabasite rocks of Loukounga. (a) Contact between paragneiss of Loukoula and amphibolite of Nemba Complex; (b) Folded amphibolite showing a small thrust movement; (c) lenticulars gabbro boulders within cleavage fine greenschists; (d) alternating micaschists and fine greenschists.

4.2. Microscopic Description

Metabasites rocks of Loukounga are studied on fine sections and some examples presented in **Figure 5**.

Metagabbros are represented by samples Louk 30b (**Figure 5(e)**) and Louk 32 (**Figure 5(f)**). They are made of actinote, hornblende, epidote, plagioclase, sphene, pyroxene, zircon and rare opaque. The pyroxenes are pseudomorphozed on green amphibole which line plagioclase crystals relics. Plagioclases are often saussuritized on epidote and locally contain epidote, quartz and calcite intrusions. The textures are varied from nematogranoblatic, lepidogranoblastic to lepidoblastic.

Epidotites are made of pistachite, plagioclase, chlorite, biotite, pyroxene, actinote and opaque minerals (**Figure 5(g)**, **Figure 5(h)**) in variable proportions. They contain veins or amygdales composed of epidote, quartz, calcite and chloritized biotite, often oriented along schistosity. Epidote is either in fine crystals either in porphyroclastes moulded in the schistosity. The textures observed are

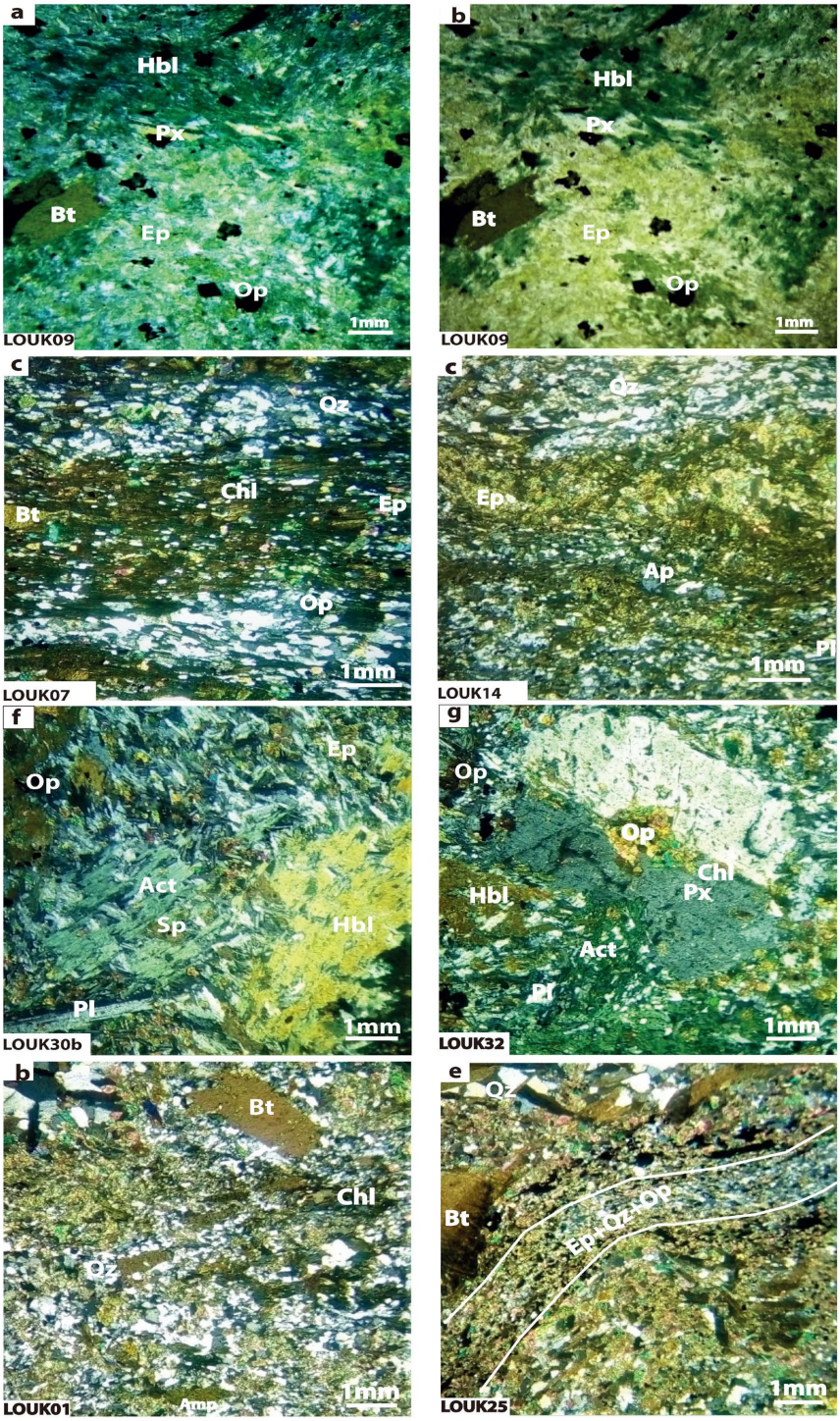

Figure 5. Microscopic pictures from metabasite rocks of Loukounga. Amphibolites ((a) Louk 09, (b) Louk 20); greenschists ((c) Louk07, (d) Louk 14); metagabbros ((e) Louk 30b, (f) Louk 32); Epidotite ((g) Louk 01, (h) Louk 25): Act-actinote, Pl-plagioclase, Ep-epidote, Chl-chlorite, Bt-biotite, Qz-quartz, Hbl-hornblende, Sp-spinel, Ap-apatite, Px-pyroxene, Op-opaque.

granoblastic and grano-lepidoblastic and in some places it becomes mylonite type.

4.3. Geochemistry and Petrographic Classification

26 samples from metabasites of Loukounga are analysed and their results presented in Table 1. Major elements give value SiO_2 (41.85% - 58.23%), Al_2O_3 (13.35% - 19.14%), MgO (2.03% - 7.11%), CaO (4.13% - 12.61%), Na_2O (0.45% - 6.68%) and TiO_2 (1.07% - 2.69%).

Table 1. (a) Analytical results of major elements and trace elements of samples of epidotite, amphibolite and shales (3 samples); (b) Analytical results of major elements and trace elements of the samples from the shales (7 samples) and the metagabbros.

(a)

Simple No	LO01	LO08	LO25	LO06	LO03a	LO04	LO45	LO11	LO02	LO2a	LO12a	LO12b	LO16
	Epidotite						Amphibolite					Schist	
SiO_2	47.25	48.11	49.76	51.26	46.68	42.37	48.38	50.97	51.94	52.15	42.04	45.61	49.07
Al_2O_3	19.14	17.02	15.19	14.98	18.39	17.43	16.48	16.74	16.45	16.54	16.64	14.88	16.73
Fe_2O_3	11.17	11.54	14.97	12.87	11.65	14.54	10.46	9.89	9.49	9.44	15.62	16.47	10.34
MnO	0.18	0.27	0.36	0.37	0.19	0.25	0.23	0.18	0.17	0.17	0.27	0.20	0.20
MgO	3.88	3.41	2.03	3.16	5.82	6.97	7.08	6.47	6.03	5.96	4.74	5.47	5.59
CaO	9.50	11.81	11.12	11.82	7.27	10.33	5.70	6.33	6.44	6.59	10.63	6.55	6.11
Na_2O	4.00	2.40	1.46	0.57	4.09	2.46	4.81	5.06	5.18	5.22	3.00	4.56	5.64
K_2O	0.46	0.11	1.78	0.30	0.89	0.44	0.74	0.58	0.55	0.53	0.10	0.10	0.14
TiO_2	1.21	1.52	1.31	1.13	1.31	1.37	1.68	1.12	1.10	1.11	1.85	2.29	2.46
P_2O_5	0.11	0.20	0.69	0.31	0.29	0.20	0.29	0.25	0.27	0.27	0.38	0.38	0.37
PF	2.98	2.93	1.12	3.49	3.09	3.33	3.09	2.77	2.50	2.18	3.95	2.63	2.84
Total	99.88	99.33	99.79	100.24	99.68	99.67	98.93	100.34	100.12	100.16	99.21	99.13	99.49
As	2.32	1.98	0.86	2.41	1.50	2.56	0.62	0.59	1.01	0.98	1.23	0.85	0.88
Ba	144	91.7	491	163	357	148	450	213	203	193	74.9	17.5	40.8
Be	0.25	0.55	1.17	0.54	0.29	0.56	1.28	0.54	0.59	0.55	0.40	0.85	1.00
Bi	0.05	0.08	0.20	1.17	0.05	0.06	0.5	0.5	0.5	0.16	0.05	0.5	0.5
Cd	0.11	0.24	0.48	0.61	0.12	0.14	0.34	0.15	0.14	0.13	0.20	0.10	0.12
Co	40.6	39.7	23.4	16.8	42.0	53.3	38.4	39.7	36.8	36.1	45.4	51.8	52.7
Cr	90.7	80.6	6.2	37.2	69.1	85.4	213	58.4	56.6	57.4	94.1	102	56.9
Cs	0.31	0.06	1.40	0.19	0.50	0.32	0.49	0.30	0.28	0.27	0.05	0.04	0.07
Cu	13.9	6.0	7.9	27.6	7.6	10.4	3.7	0.5	4.1	6.3	5.6	2.1	0.5
Ga	20.8	26.7	26.4	26.8	21.3	24.5	19.8	17.2	16.3	16.4	25.4	18.4	21.7
Ge	2.51	2.89	3.88	3.71	2.20	2.62	2.10	1.83	1.76	1.89	2.83	1.92	2.10
Hf	2.61	5.46	6.54	5.02	3.73	3.40	9.56	3.09	3.20	3.24	3.09	3.56	4.58
In	0.08	0.13	0.12	0.16	0.10	0.10	0.11	0.08	0.07	0.08	0.11	0.07	0.11
Mo	0.74	0.5	0.5	0.62	0.5	0.64	0.5	0.5	0.5	0.5	0.53	0.5	0.5
Nb	7.23	19.9	11.3	11.1	9.02	7.98	28.4	7.48	7.18	7.26	15.3	18.0	17.2
Ni	120	70.8	15.0	36.2	98.3	111	161	75.3	72.8	70.5	73.3	73.9	71.7

Continued

Pb	56.6	41.9	187	66.8	40.8	50.4	47.7	22.0	22.6	24.0	25.1	13.3	17.6
Rb	14.1	4.48	48.1	9.45	23.7	11.5	19.8	14.7	14.1	13.6	2.93	1.76	2.54
Sb	0.90	0.80	0.58	0.68	0.70	0.86	0.65	0.43	0.43	0.48	0.70	0.63	0.73
Sc	31.99	23.47	59.84	32.85	44.59	38.74	34.33	37.24	37.01	38.01	30.67	33.47	34.56
Sn	1.37	2.42	2.14	1.31	1.19	1.29	3.30	0.73	0.84	0.87	1.35	1.07	1.36
Ta	723	915	468	637	391	454	176	234	233	252	760	322	304
Sr	0.49	1.37	0.80	0.71	0.66	0.56	2.20	0.54	0.51	0.53	0.95	1.17	1.15
Th	0.84	4.00	9.71	3. 39	1.54	1.40	1.81	1.22	1.24	1.28	1.81	2.20	3.74
U	0.36	0.79	1.82	0.49	0.35	0.29	0.44	0.64	0.57	0.60	0.31	0.32	0.51
V	106	208	369	208	184	218	157	139	134	133	250	228	152
Y	29.8	43.5	52.0	38.5	33.0	30.7	52.9	27.8	27.7	28.7	35.2	34.0	38.5
Zn	113	135	251	396	175	202	229	156	147	147	140	137	177
Zr	110	196	248	199	141	127	403	121	120	122	125	139	181
La	13.0	29.5	51.2	38.9	23.2	21.7	29.1	19.4	19.9	20.9	25.0	20.9	29.2
Ce	25.8	61.1	104	72.4	45.7	41.2	71.6	37.3	38.5	40.2	50.0	43.7	61.6
Pr	3.52	7.65	12.3	8.34	5.54	5.03	10.3	4.55	4.70	4.91	6.33	5.42	7.54
Nd	15.5	32.9	49.0	34.3	23.5	21.2	46.6	19.1	20.2	20.9	26.4	23.1	31.8
Sm	4.19	7.87	10.3	7.43	5.65	5.16	11.7	4.63	4.80	4.93	5.95	5.59	7.55
Eu	1.51	2.31	2.72	2.39	2.06	1.83	3.37	1.64	1.56	1.64	2.37	1.78	2.49
Gd	4.59	7.86	9.75	7.44	5.84	5.42	10.5	4.81	4.79	4.98	6.17	5.67	7.48
Tb	0.795	1.26	1.55	1.15	0.990	0.879	1.70	0.807	0.831	0.854	0.966	0.940	1.20
Dy	4.98	7.99	9.62	7.16	6.34	5.71	10.3	5.13	5.28	5.36	6.18	6.09	7.58
Ho	1.06	1.68	2.09	1.50	1.31	1.18	2.06	1.07	1.08	1.12	1.30	1.29	1.56
Er	2.87	4.39	5.44	3.94	3.51	3.07	5.38	2.89	2.92	2.96	3.47	3.62	4.08
Tm	0.404	0.620	0.770	0.547	0.493	0.423	0.740	0.391	0.399	0.419	0.468	0.517	0.557
Yb	2.63	4.12	5.10	3.65	3.16	2.81	4.87	2.64	2.65	2.67	3.13	3.57	3.68
Lu	0.401	0.623	0.764	0.556	0.488	0.425	0.701	0.406	0.410	0.412	0.494	0.545	0.551
Nb/Th	8.63	4.98	1.16	3.27	5.87	5.71	15.65	6.13	5.81	5.69	8.19	4.59	1.69
Nb/La	0.56	0.67	0.22	0.29	0.39	0.37	0.98	0.39	0.36	0.35	0.86	0.59	0.31
Zr/Y	3.69	4.5	4.78	5.17	4.28	4.14	7.62	4.33	4.35	4.23	4.08	4.7	4.56
Zr/Nb	15.22	9.85	22.06	17.97	15.65	15.92	14.17	16.11	16.78	16.75	7.71	10.5	16.61
Th/Ta	1.71	2.91	12.1	4.74	2.32	2.49	0.89	2.24	2.41	2.43	1.88	3.24	7.93
Nb/Y	0.24	0.46	0.22	0.29	0.27	0.26	0.54	0.27	0.26	0.25	0.53	0.45	0.27
Sm/Y	0.14	0.18	0.2	0.19	0.17	0.17	0.22	0.17	0.17	0.17	0.16	0.2	0.19
La/Nb	1.8	1.48	4.55	3.5	2.58	2.72	1.02	2.59	2.77	2.88	1.16	1.7	3.23
Th/La	0.06	0.14	0.19	0.09	0.07	0.06	0.06	0.06	0.06	0.06	0.11	0.13	0.18

(b)

Sample No	Lo29b	Lo18b	Lo22	Lo26a	Lo28	Lo23	Lo07	Lo18a	Lo37	Lo09	Lo42	Lo30	Lo32
	Schist							metagabbro					
SiO_2	51.23	49.63	56.99	58.23	42.08	47.80	48.91	41.85	46.23	46.47	48.97	53.86	57.77
Al_2O_3	14.02	15.16	15.36	13.35	15.84	13.89	16.91	16.79	18.16	15.18	16.83	15.78	14.16
Fe_2O_3	14.65	13.33	8.82	11.32	17.70	16.39	10.24	15.66	11.28	13.00	10.81	8.55	6.85
MnO	0.36	0.20	0.15	0.22	0.36	0.25	0.25	0.31	0.36	0.23	0.21	0.19	0.20
MgO	2.74	5.34	3.55	2.38	3.03	5.43	4.38	5.80	4.96	6.18	7.11	4.48	4.70
CaO	10.34	6.67	4.13	8.76	10.72	6.40	7.00	12.61	9.80	9.05	4.77	7.31	6.46
Na_2O	0.82	4.47	6.06	2.07	2.15	3.87	5.07	0.45	4.08	3.96	5.63	6.13	6.68
K_2O	1.62	0.11	0.60	0.14	0.53	0.15	0.54	0.13	0.09	0.22	0.16	0.15	0.25
TiO_2	1.55	1.91	2.43	1.40	2.46	2.68	2.69	1.40	1.19	1.93	1.99	1.07	1.13
P_2O_5	0.58	0.35	0.19	0.31	0.83	0.20	0.24	0.24	0.30	0.64	0.40	0.17	0.29
PF	1.77	2.73	1.81	2.10	3.42	2.51	3.69	3.82	2.98	2.98	3.26	1.36	1.06
Total	99.67	99.90	100.09	100.28	99.11	99.56	99.91	99.05	99.43	99.83	100.12	99.04	99.54
As	1.46	0.87	0.55	2.43	5.24	1.16	1.43	2.98	0.93	1.82	0.89	0.85	0.85
Ba	50	39.3	181	57.0	245	270	203	124	119	67.0	46.7	33.7	89.2
Be	1.11	1.08	0.77	0.51	0.70	1.70	0.60	0.90	0.69	0.78	0.65	0.91	0.94
Bi	0.10	0.5	0.5	0.10	0.11	0.06	0.63	0.5	0.5	0.5	0.07	0.5	0.5
Cd	0.41	0.11	0.11	0.15	0.39	0.32	0.64	0.20	0.19	0.11	0.11	0.10	0.16
Co	30.9	49.8	30.9	27.4	14.0	56.1	34.9	58.6	43.3	50.5	57.1	32.8	29.8
Cr	12.0	55.0	16.2	17.3	10.7	26.7	75.2	54.5	66.6	80.2	81.1	62.7	51.4
Cs	1.28	0.06	0.43	0.13	0.28	0.10	0.40	0.14	0.08	0.10	0.10	0.07	0.02
Cu	28.6	2.4	3.8	38.9	67.8	6.1	50.4	3.0	2.3	6.9	2.1	2.4	3.0
Ga	25.9	20.6	19.1	25.4	27.6	21.7	19.1	30.9	25.5	23.2	18.3	16.5	11.6
Ge	3.59	2.30	1.76	2.91	3.68	2.44	2.01	3.58	2.44	2.24	1.56	2.05	1.53
Hf	5.27	3.39	4.31	3.11	8.52	3.98	3.92	3.33	2.31	3.41	3.94	2.41	2.67
In	0.11	0.09	0.09	0.09	0.12	0.10	0.09	0.10	0.08	0.08	0.06	0.06	0.03
Mo	0.53	0.5	0.5	1.51	1.59	0.5	0.89	0.5	0.5	0.5	0.53	0.5	0.5
Nb	12.3	13.0	13.7	10.3	23.2	14.0	15.7	10.6	4.77	20.4	7.28	4.67	4.81
Ni	26.0	68.4	33.8	30.4	18.4	62.9	58.4	85.7	146	80.0	177	124	154
Pb	16	18.3	19.6	57.3	115	35.9	23.6	31.5	60.7	26.2	25.8	39.0	31.3
Rb	45.3	2.70	16.2	5.74	12.1	6.38	17.2	5.43	2.57	5.49	4.25	3.01	2.93
Sb	0.67	0.67	0.73	0.87	0.75	1.10	0.70	0.64	1.15	1.06	0.96	0.71	0.66
Sc	51.24	36.66	34.72	30.96	64.93	46.80	38.34	23.65	21.93	31.73	29.09	23.64	20.93
Sn	2.27	1.38	1.70	2.08	2.40	1.98	1.42	1.22	1.01	1.02	1.29	0.94	1.00
Ta	482	403	203	539	558	340	220	902	725	555	217	540	266
Sr	0.92	0.84	1.01	0.83	2.05	0.98	1.00	0.75	0.29	1.12	0.47	0.29	0.30

Continued

Th	7.29	1.65	1.30	2.71	12.3	1.39	1.50	2.32	0.47	2.19	0.81	0.57	0.53
U	1.45	0.30	0.28	0.67	2.04	0.31	0.28	0.37	0.13	0.45	0.15	0.11	0.09
V	362	231	194	268	380	320	220	204	247	220	206	159	137
Y	44.9	32.4	33.4	31.3	53.5	35.1	36.4	28.3	25.3	27.9	29.1	21.2	17.3
Zn	271	161	156	106	208	245	472	202	252	158	371	190	201
Zr	205	131	158	119	331	148	152	129	87.8	140	151	97.3	105
La	39.7	19.7	18.5	25.4	59.7	19.9	18.1	24.6	16.4	27.1	19.3	15.8	13.8
Ce	81.8	42.5	39.4	52.0	124	42.2	36.9	51.5	34.8	53.7	42.1	33.8	29.1
Pr	9.74	5.45	5.27	6.37	14.5	5.76	4.75	6.22	4.45	6.41	5.41	4.30	3.79
Nd	39.1	23.5	23.0	26.0	57.1	26.2	20.9	25.7	19.2	26.2	22.8	18.4	15.5
Sm	8.37	5.83	5.69	5.70	11.7	6.37	5.54	5.83	4.40	5.61	5.42	4.21	3.62
Eu	2.30	1.99	2.08	1.74	2.75	2.21	2.01	2.17	1.77	2.26	1.55	1.39	0.977
Gd	7.95	5.84	5.72	5.48	10.6	6.18	5.87	5.79	4.42	5.47	5.22	4.16	3.39
Tb	1.27	0.952	0.950	0.874	1.68	1.03	1.01	0.928	0.715	0.839	0.862	0.671	0.543
Dy	8.11	5.94	6.03	5.53	10.5	6.46	6.58	5.59	4.52	5.28	5.38	4.02	3.35
Ho	1.72	1.28	1.33	1.19	2.14	1.42	1.40	1.13	0.942	1.10	1.14	0.826	0.684
Er	4.73	3.28	3.53	3.15	5.75	3.72	3.76	2.92	2.48	2.85	3.02	2.10	1.85
Tm	0.662	0.471	0.514	0.443	0.834	0.529	0.524	0.390	0.333	0.398	0.419	0.283	0.259
Yb	4.38	3.17	3.40	3.03	5.48	3.51	3.54	2.56	2.21	2.66	2.73	1.86	1.72
Lu	0.678	0.470	0.487	0.449	0.856	0.511	0.508	0.386	0.338	0.399	0.399	0.276	0.264
Nb/Th	7.91	10.56	3.79	1.88	10.08	10.49	4.13	10.16	10.01	9.3	8.98	8.24	9.1
Nb/La	0.66	0.74	0.4	0.39	0.71	0.87	0.39	0.29	0.3	0.75	0.38	0.3	0.35
Zr/Y	4.05	4.74	3.81	6.19	4.21	4.18	3.88	3.47	4.5	5.04	5.2	4.59	6.09
Zr/Nb	10.07	11.55	11.66	14.26	10.53	9.68	8.18	18.42	9.52	6.88	20.78	20.83	21.85
Th/Ta	1.96	1.28	3.26	6	1.42	1.51	4	1.6	1.5	1.95	1.72	1.96	1.78
Nb/Y	0.4	0.41	0.33	0.43	0.4	0.43	0.48	0.19	0.8	0.73	0.25	0.22	0.28
Sm/Y	0.18	0.17	0.18	0.22	0.18	0.15	0.19	0.17	0.2	0.2	0.19	0.2	0.21
La/Nb	1.51	1.35	2.48	2.57	1.42	1.15	2.59	3.43	2.31	1.33	2.65	3.38	2.87
Th/La	0.08	0.07	0.11	0.21	0.07	0.08	0.09	0.03	0.06	0.08	0.04	0.04	0.04

The Mg# colour index [34] is comprised between 16.2% and 43.6%. The TiO_2 concentration based of [35] [36] and [37] classifications give 19 samples with low Ti (TiO < 2) and 6 samples with high Ti (TiO > 2).

The Harker diagrams (**Figure 6**) of mobile elements as Na, K, LILE, and Pb used to detect influence of weathering or low-grade metamorphism in the samples show a bad correlation between major and traces elements. In contrast, the high field strength elements (HFSE) relatively motionless define linear trends in binary element diagrams.

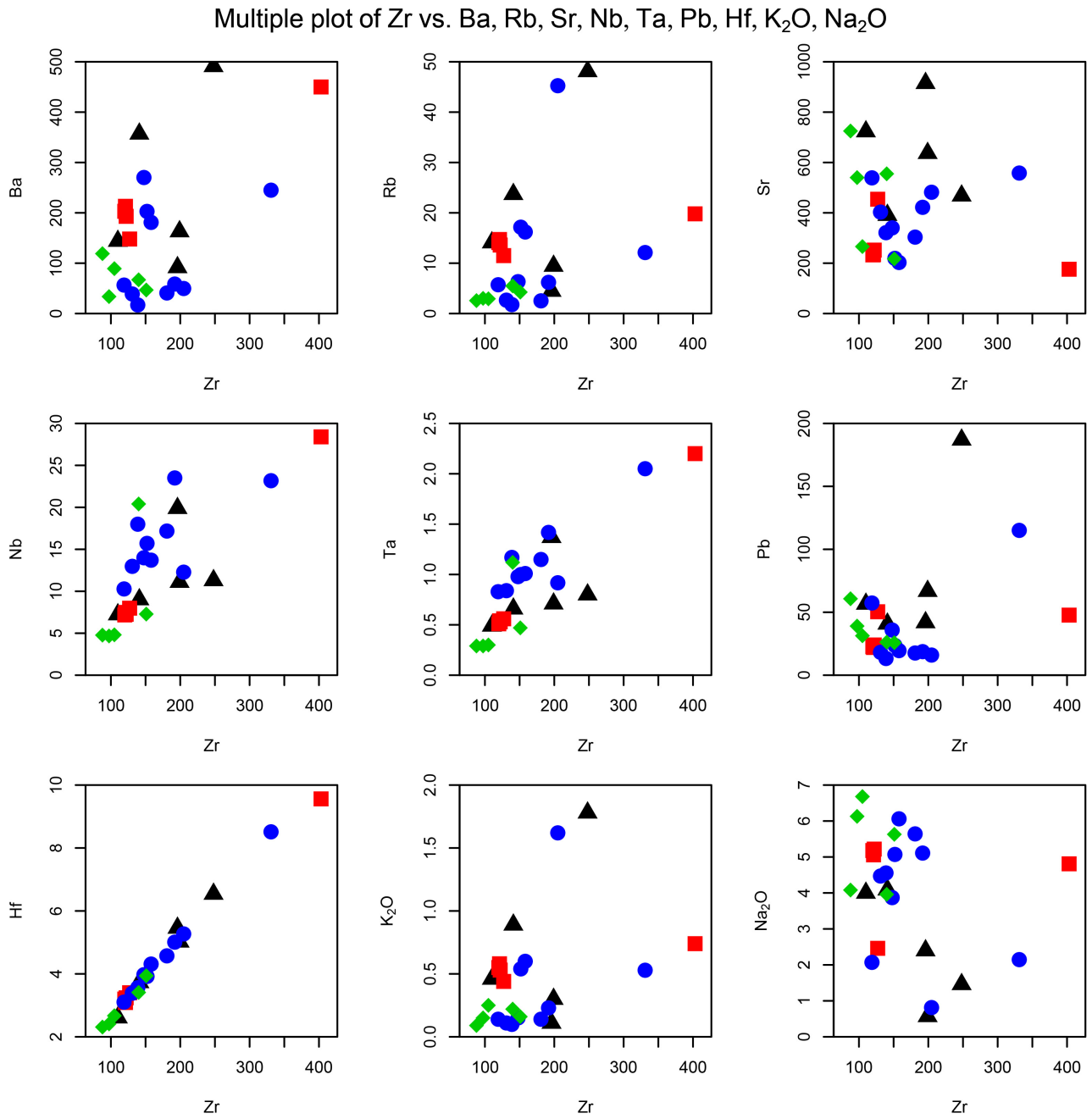

Figure 6. Harker diagrams showing bad correlation between mobile elements and rare earth elements and a positive correlation of the HFSE elements of metabasite rocks of Loukounga. The abscissa axis (x) corresponds to the Zr content taken as an index of magmatic differentiation. The ordinate axis (y) corresponds to the contents of oxides and other trace elements. The oxides are expressed in % weight and the trace elements are expressed in ppm.

Zr/Ti-Nb/Y diagram of [38] modified by [39] (**Figure 7**) place samples in basalts and andesitic basalts fields. The Zr/Y < 4.5 ratio of the greenschists and epidotites indicate a tholeiitic basalt and the Zr/Y > 4.5 ratio of the amphibolites and metagabbros place the rocks in transitional basalt. The Nb/Y < 1.0 ratio correspond of that of a subalkaline rock.

The composition of incompatibles traces elements is illustrated in binary

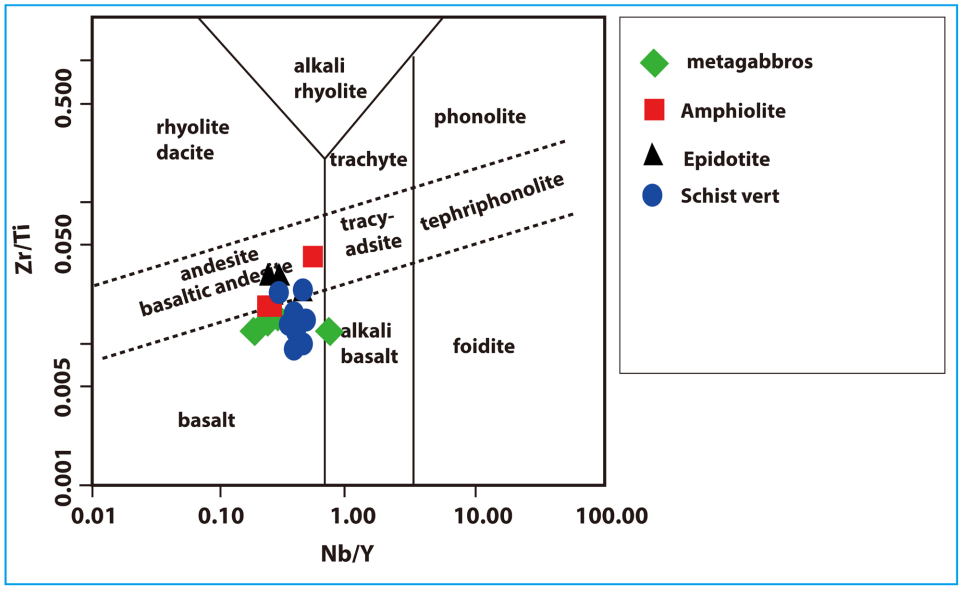

Figure 7. Classification of metabasites rocks of Loukounga in Nb/Y-Zr/Ti diagram of [38] [39]. Samples fall in basalt, andesite and basaltic andesite.

diagrams normalized to chondrites and primitive mantle (**Figure 8**). Rare earth spectra of Loukounga lava normalized to Nakamura [40] chondrites (**Figure 8(a)**) are subparallel in shape at HREE and slightly concave downwards at MREE and some samples show weak negative Eu anomalies (Eu/Eu* = 0.83 - 0.99) and others on the other hand showing more positive anomalies in Eu (Eu/Eu* = 1.01 - 1.11). All samples are enriched in LREE and are characterized by steeper REE slopes than E-MORB (LaN/YbN: 3.67 à 6.77). Total REE concentrations are consistently higher in all lavas than MORBs (∑REE: 78.85 à 264.60).

The normalized spectrum to the N-MORB of [41] (**Figure 8(b)**) is marked by a selective enrichment in LILE (Cs, Ba, Sr) compared to HSFE (Zr, Nb, Th, Y) and contains a strong positive Pb anomaly and a negative Nb, K, Zr and Ti anomalies. The normalized spectrum to the primitive mantle of [42] shows enrichment in LILE and HFSE elements (**Figure 8(c)**). The anomaly is slightly negative for Ta-Nb and Ti and strongly positive for Pb.

Traces elements are used to determine geological context. The Zr/Y-Zr diagram of Pearce and Norry [43] place the rocks in within plate basaltic lavas, except two rocks which located to the limit of MORB field (**Figure 9**). The Zr/Y > 1.5 attribute the rocks to continental types of Pearce [44].

Zr-Th-Nb triangular diagram of Wood [45] and Nb-Zr-Y triangular diagram of Meschede [46] place samples in wide fields from the MORB, WPT, CAB and Alkaline basalt to arc basalt (**Figure 10**).

Plotted in Th/Ta-Tb/Ta diagram of [47] [48] used on the metabasites rocks of the Mayombe of Gabon, samples are concentrated in CFB field (**Figure 11**).

Plotted in Th/Ta-Tb/Ta diagram of [47] [48] used on the metabasites rocks of the Mayombe of Gabon, samples are concentrated in CFB field (**Figure 11**).

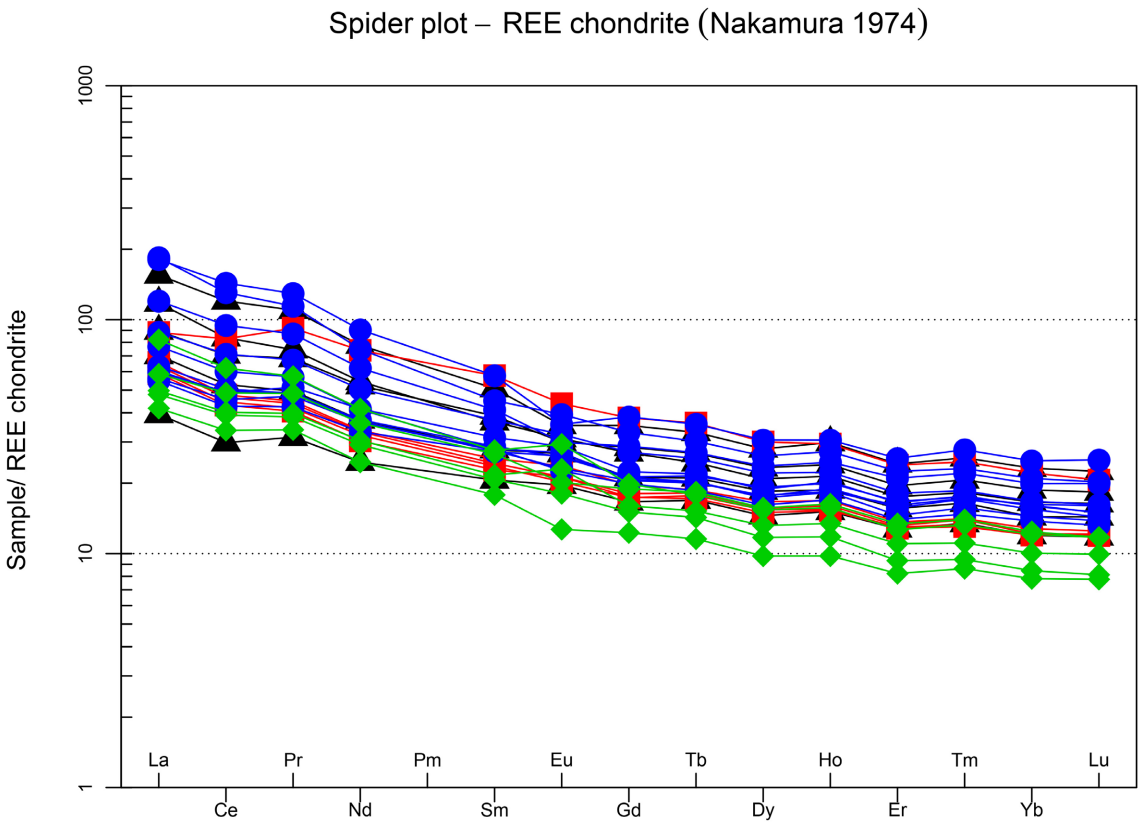
Spider plot – REE chondrite (Nakamura 1974)
Sample/ REE chondrite
1000
100
10
1
La
Ce
Pr
Nd
Pm
Sm
Eu
Gd
Tb
Dy
Ho
Er
Tm
Yb
Lu

(a)

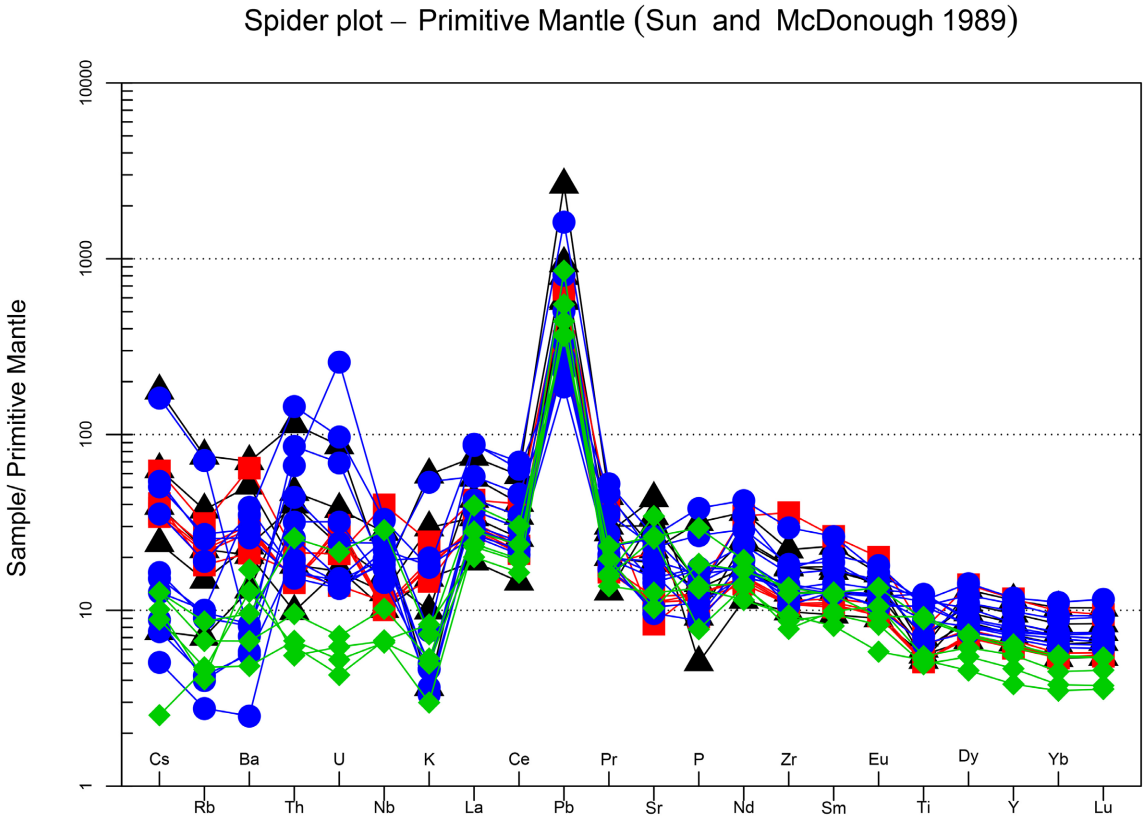
Spider plot – Primitive Mantle (Sun and McDonough 1989)
Sample/ Primitive Mantle
10000
1000
100
10
1
Cs
Rb
Ba
Th
U
Nb
K
La
Ce
Pb
Pr
Sr
P
Nd
Zr
Sm
Eu
Ti
Dy
Y
Yb
Lu

(b)

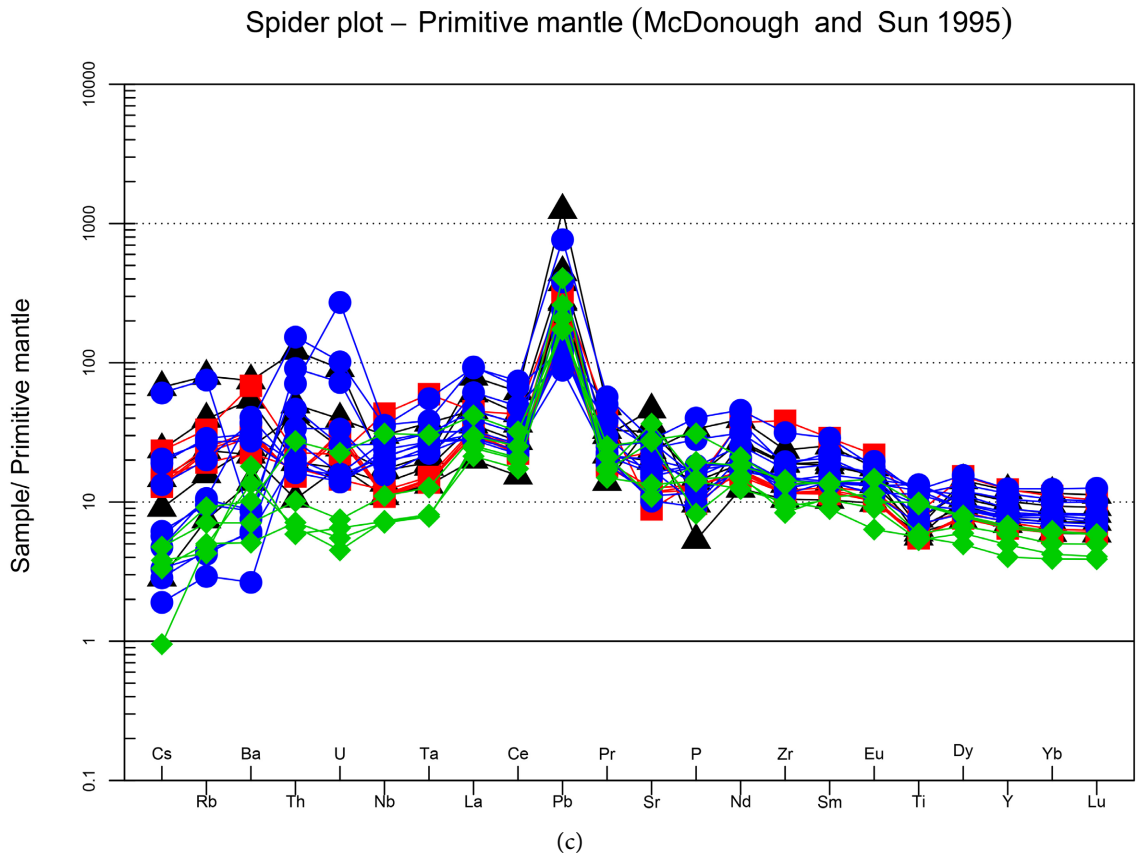

Figure 8. (a) Sper diagram of REE Loukounga métabasites normalized to the chondrites of [40]; (b) Sper diagram of traces-element of Loukounga métabasites normalized to the NMORBS of Sun and Mc Donough [41]; (c) Speder diagram of traces-element of Loukounga métabasites normalized to the primitive mantle of [42].

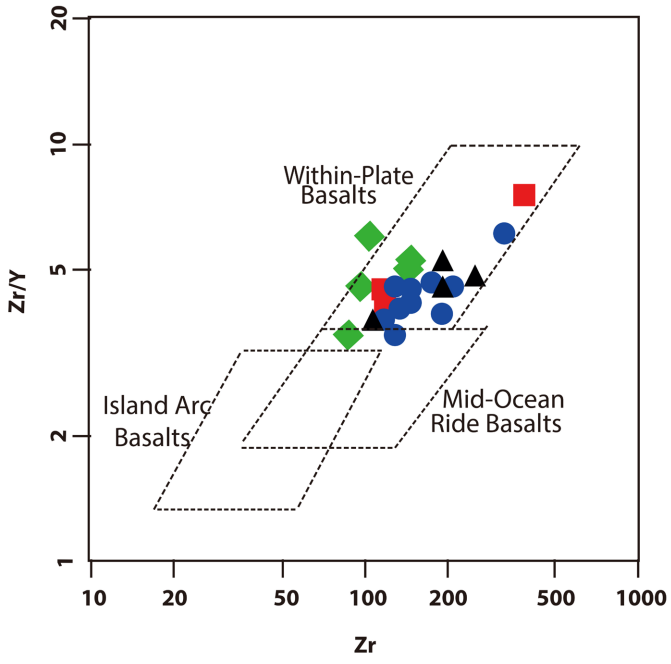

Figure 9. Characterization of geodynamic context of metabasites of Loukounga in Zr/Y-Zr diagram of [43].

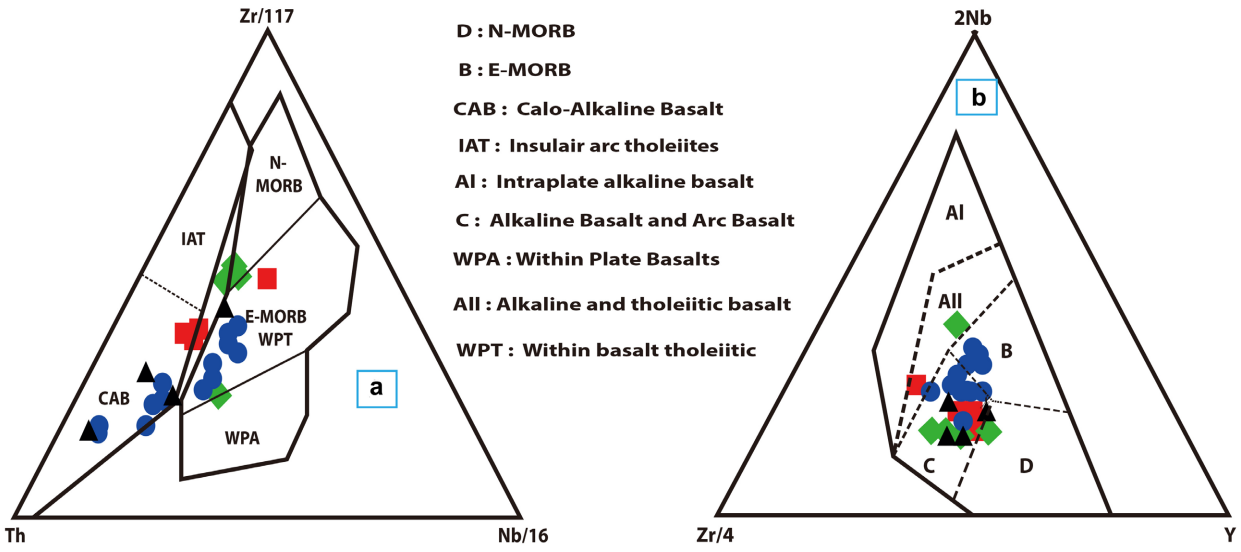

Figure 10. Plot of metabasite rocks of Loukounga river in triangular diagrams (a) of [45] (b) of [46]: in Zr-Th-Nb diagram, samples fall in CAB, E-MORB and N-MORB; in Nb-Zr-Y diagram, samples characterize dominantly the alkaline basalt and arc basalt with a few samples in E-MORB and N-MORB and alkaline with tholeiitic basalts.

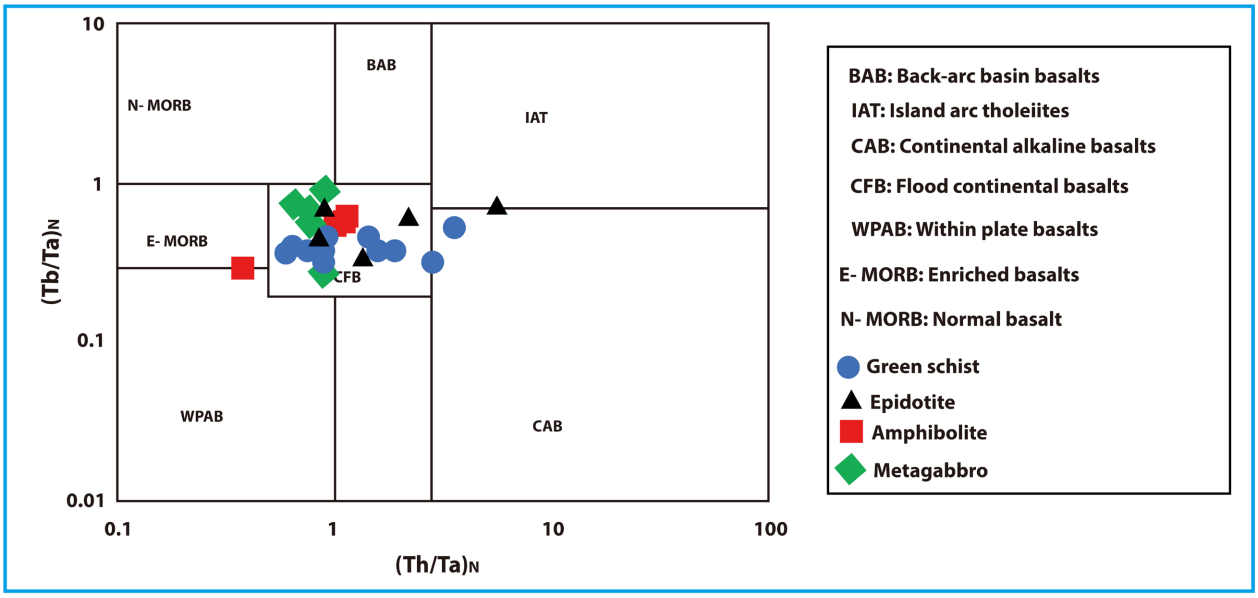

Figure 11. Plots of Loukounga metabasite samples in [47] and [48] diagram. The majority of samples fall in CFB context with one sample in the CAB context, two samples at the limit and one sample at the limit of WPAB and E-type MORB.

5. Discussion

The metabasites of Loukounga are attached to the Nemba Complex of the neoproterozoic Mayombe belt which is made of metagabbros, metabasalts, amphibolites and greenschists and dated in Congo at 915 ± 8 Ma by U-Pb zircon [11] and between 999 ± 7 Ma and 920 ± 8 Ma, in RDC [6] from the Gangila basic rocks.

5.1. Petrogenesis

Metabasites samples of Loukounga are ranged macroscopically in amphibolites,

metagabbros epidotites and greenschists facies. Fine sections show a hydrothermal overprint marked by: 1) a zoned vacuoles filled with epidote, quartz and chlorite which successively crystallized; 2) an amygdale filled by calcite; 3) a late secondary growth of non-oriented epidote, chlorite, hornblende and quartz over older parageneses (**Figure 5**).

Geochemical of major elements shows that these rocks are basic to intermediate composition with a few samples in ultrabasic composition. The Mg# colour index [34] value indicated that they are in part felsic with differentiated magma and in part mafic with poorly differentiated magma. The Harker diagrams (**Figure 6**) show a bad correlation between major and traces elements. In contrast, the high field strength elements (HFSE) relatively motionless define linear trends in binary element diagrams indicating that their concentrations have not been affected by weathering or low-grade metamorphism.

Samples in discrimination diagrams Zr/Ti-Nb/Y of [38] modified by [39] characterized samples as basalts and andesitic basalts fields (**Figure 7**). The Zr/Y < 4.5 ratio of the greenschists and epidotites indicate a tholeiitic basalt and the Zr/Y > 4.5 ratio of the amphibolites and metagabbros place the rocks in transitional basalt. The Nb/Y < 1.0 ratio correspond of that of a subalcalin rocks.

5.2. Geodynamic Context and Magma Source

Spectra of Loukounga normalized to N-MORBS and primitive mantle [41] (**Figure 8(b)**) show enrichment in LILE and HFSE elements but with slight negative anomalies for the Nb, Ta and Ti and Sr variables anomalies. Positive anomaly is very strong for Pb, this confer a tholeiites continental character. It is comparable to those known elsewhere as in the traps of Decan [49] and Frankelin (**Figure 12**) [50].

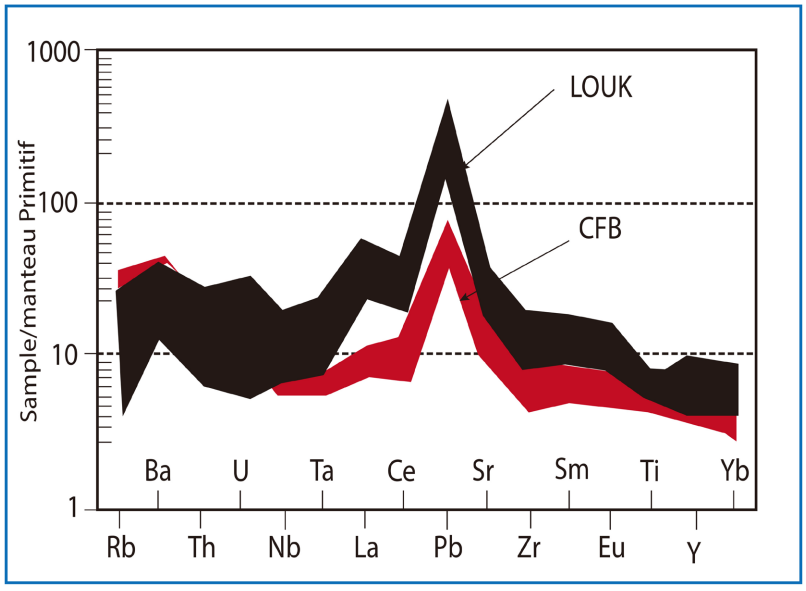

Figure 12. Diagram of comparison of multielement spectra normalized to the primitif mantle of [42] of the metabasites of Loukounga and the CFB of Frakelin [50].

The Zr/Y-Zr diagram of [43] places the rocks in within plate basaltic lavas, except two (02) rocks one of which is in the field of MORB (**Figure 9**). A tholeiitic basalts origin is detected for greenschists and epidotites with Zr/Y < 4.5, however a transitional basalts origin is considered for amphibolites and metagabbros with Zr/Y > 4.5. The Zr/Y > 1.5 attribute the rocks to continental types of [41].

Within intraplate basalts associated with E-MORB and Calco-alkaline Basalt are detected in triangular (Zr-Th-Nb) diagram of [45] (**Figure 10(a)**). The E-MORB associated with major samples plotted in alkaline basalt and arc basalt is recognized in triangular (Nb-Zr-Y) diagram of [46] (**Figure 10(b)**). The wide dispersion from within plaque basalt (WPB) to arc basalt fields is often characteristics of continental within plaque basalts particularly the traps basalts or CFB [51] like observed in Th/Ta-Tb/Ta diagram of [47] [48] (**Figure 11**) used for the metabasites rocks of the Mayombe belt in Gabon.

CFB-related lavas belong to an association of transitional tholeiitic basalts and consist of subalkaline basalt and basaltic andesite as observed at Loukounga. These basalts are characterized by slightly low Nb concentrations (7 - 42 ppm) [51]. By comparison, the Loukounga lavas have Nb contents of between 4.64 and 28.4 ppm compatible with those of continental basalts of traps type (CFB). In the RD Congo, the equivalent of the Nemba complex, the Gangila basalts of the Zadinian Group are also described as traps basalts emplaced in the context of the rift [6].

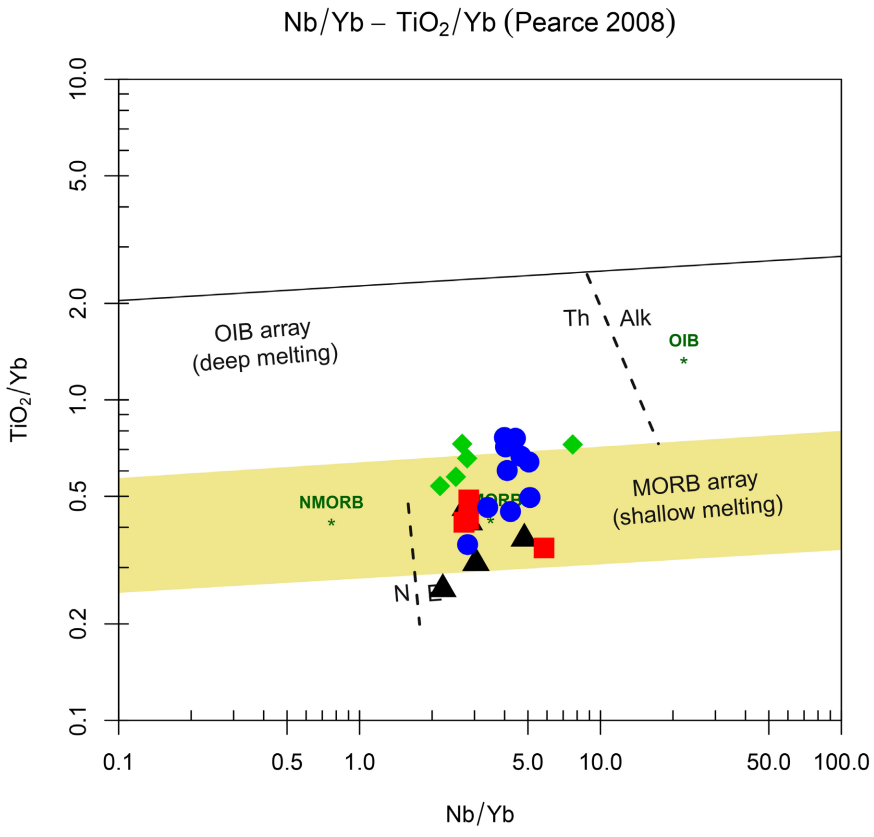

(a)

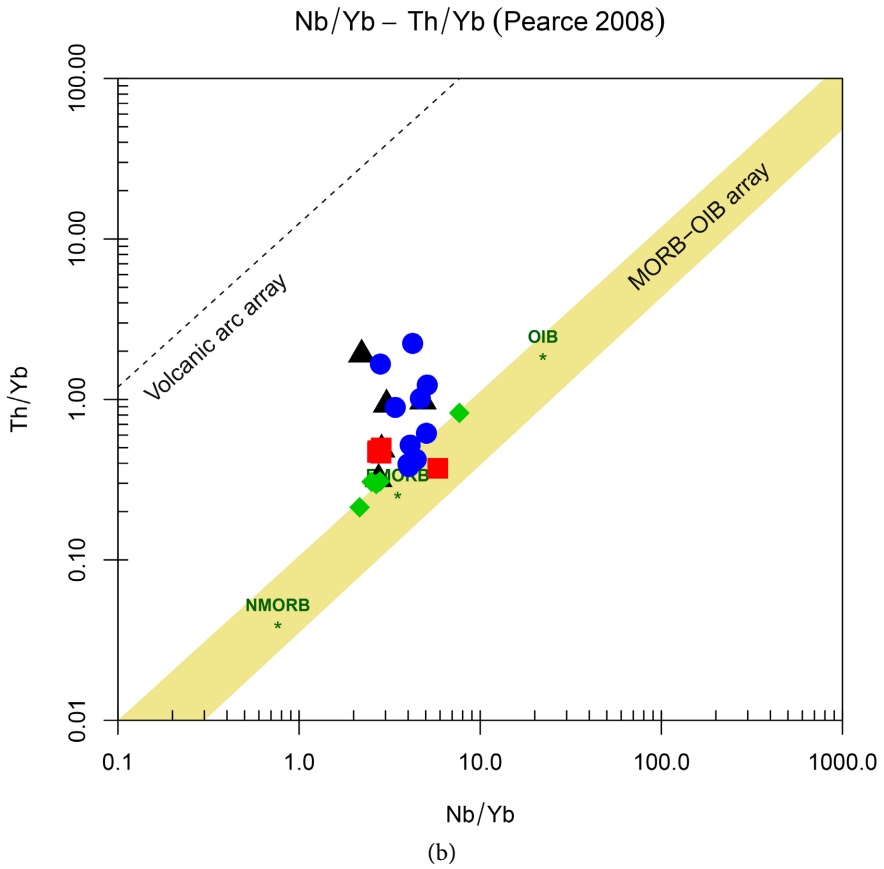

(b)

Figure 13. (a) Discrimination diagram of [55] using TiO_2/Yb-Nb/Yb ratio of Loukounga metabasites to assess magma source conditions and characterization; (b) Discrimination diagram of [55] using the Th/Yb-Nb/Yb ration of Loukounga metabasites to assess crustal contamination.

In Brazil, the Araçuaï belt hanging from the Mayombe belt, carries neoproterozoic basalts of the Macaùbas and Dom Silvério emplaced in a continental rift context [52] or associated with arc context [32] [53] [54].

To determine the source of magma, the used TiO_2/Yb-Nb/Yb diagram of [55] shows concentration of Loukounga samples in E-MORB domain and some samples in OIB array (**Figure 13(a)**) and Th/Yb-Nb/Yb show concentration dispersed around E-MORB and volcanic arc array domains (**Figure 13(b)**). These fields proximity is characteristic of mantel crustal contamination [55]. The low Zr/Nb and high (La/Yb) ratios 3.67 - 6.77 of the Loukounga tholeiitic basalts (**Table 1**) characterize an enriched atmosphere and the Nb/Y ratio between 0.22 and 0.9 shows an addition from the melting of the mantle.

The Zr/Y-Nb/Y diagram of [56] modified [57] and Nb/Th-Zr /Nb diagram of [58] (**Figure 14**) characterize a metabasalt domain derived from an enriched mantle with dispersion in PM, REC, DEP, DM fields. The geochemistry variation observed in different magma with a mantle origin is due to continental crustal contamination or the Subcontinental lithosphere as suggested also [11] [14].

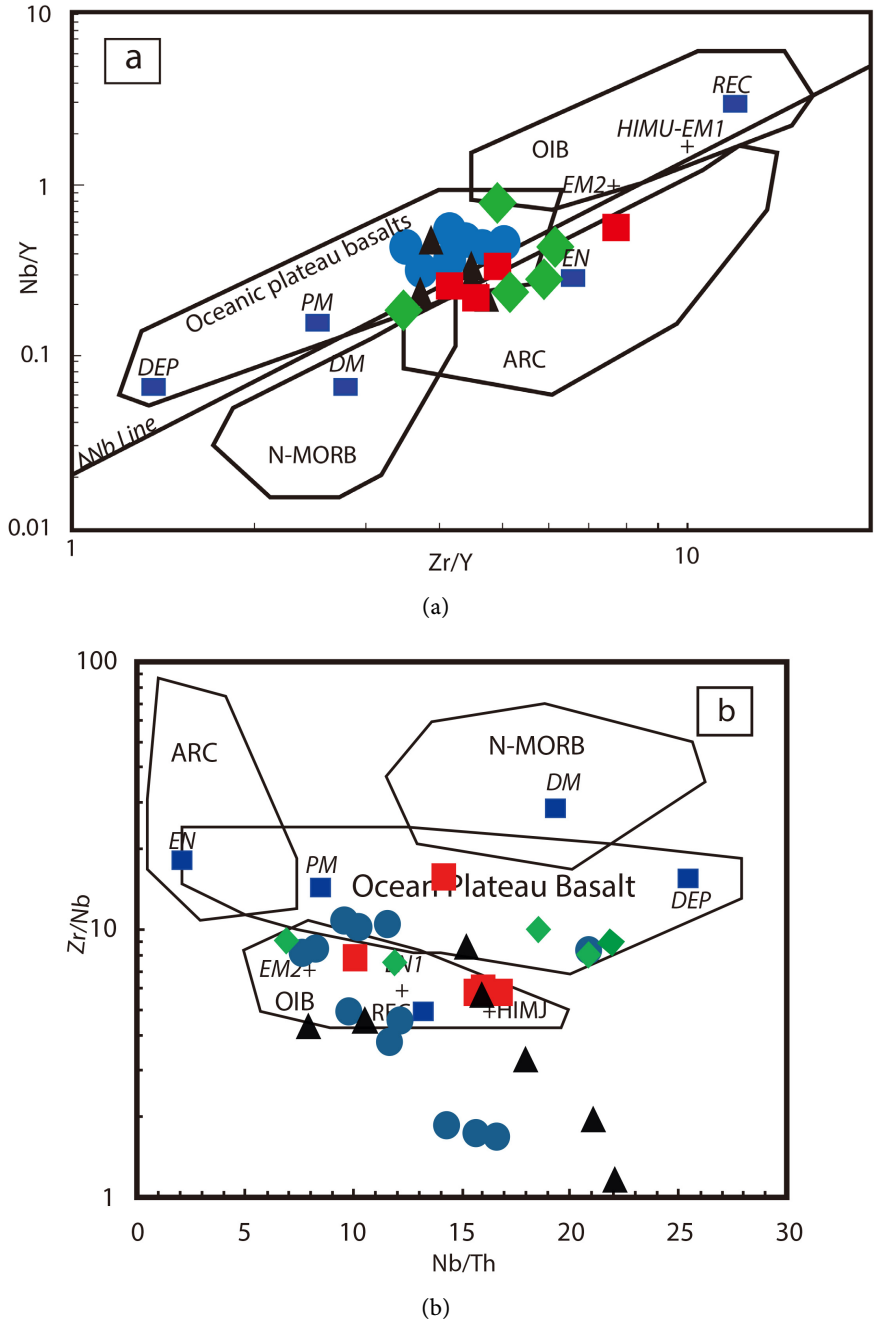

Figure 14. Discrimination diagram using immobile (HFSE) elements ratios of Loukounga metabasites to assess magma source: (a) Nb/Y-Zr/Y of [56] modified by [57]; (b) Zr/Nb-Nb/Th of [58]. Abbreviations: OIB = Oceanic Island Basalts; ARC = Magmatic Arc basalt; N-MORB = Normal Mid-Oceanic Ridge Basalts; REC = Recycled Component; PM = Primitive Mantle; HIMU-EM1 = Enriched mantle I; EM2 = Enriched Mantle 2; DEP = Depleted Plume; DM = Depleted Mantle; EN= Enriched Component.

6. Conclusion

Four groups represented by neoproterozoic metagabbro, amphibolite, epidotite and chloritoschiste are identified in the Loukounga River. Rocks affected by hydrothermal alteration bear zoned vacuoles filled with epidote, quartz and chlo-

rite which have successively crystallized. Geochemical discrimination classifies rocks in the fields of basalts and basaltic andesites. They are CFB-type basalt emplaced in an intraplate context associated with episodes of intracontinental extension as suggested [11] [14]. The incompatible elements suggest a deep mantle origin of the magma which is contaminated by continental lithosphere during its ascent.

Acknowledgements

We would like to thank MAC Congo for providing a vehicle for the field mission and the National Institute for Research in Exact and Natural Sciences (IRSEN) of Congo for its financial allocation.

Conflicts of Interest

The authors declare no conflicts of interest regarding the publication of this paper.

References

[1] Dévigne, J.P. (1959) Le Précambrien du Gabon occidental en Afrique Equatoriale Française et les régions limitrophes. Thèse Université de Clermond-Ferrand, Bulletin, Direction des Mines et de Géologie. A.E.F., n° 11, 315 p.

[2] Schermerhorn, L.J.G. and Stanton, W.I. (1963) Noticia explicativa da Carta geologica de Angola. Instituto Investigação Cientifica, Luanda, 6-15.

[3] Dadet, P. (1969) Notice explicative de la carte géologique de la République du Congo Brazzaville au 1/500,000e (zone comprise entre les parallèles 2˚ et 5˚ sud). Éditions BRGM, Vol. 70.

[4] Boudzoumou, F. and Trompette, R. (1988) La chaîne panafricaine ouest-congolienne au Congo (Afrique Equatoriale): Un socle polycyclique charrié sur un domaine subautochtone formé par l'aulacogène du Mayombe et le bassin de l'Ouest-Congo. *Bulletin de la Société Géologique de France*, **4**, 889-896. https://doi.org/10.2113/gssgfbull.IV.6.889

[5] Maurin, J.C, Boudzoumou, F., Djama, L.M., Gioan, P., Michard, A., Mpemba-Boni, J., Peucat, J.J., Pin, C. and Vicat, J.P. (1991) La chaîne protérozoïque ouest-congolienne et son avant-pays au Congo: Nouvelles données géochronologiques et structurales, implications en Afrique centrale. *Compte Rendu de l'Académie des Sciences de Paris*, *II*, **312**, 1327-1334.

[6] Tack, L., Wingate, M.T.D., Liégeois, J.P., Fernandez-Alonso, M. and Deblond, A. (2001) Early Neoproterozoic Magmatism (1000-910 Ma) of the Zadinian and Mayumbian Groups (Bas-Congo): Onset of Rodinia Rifting at the Western Edge of the Congo Craton. *Precambrian Research*, **110**, 277-306. https://doi.org/10.1016/S0301-9268(01)00192-9

[7] Thiéblemont, D., Castaing, C., Billa, M., Bouton, P. and Préat, A. (2009) Notice explicative de la carte géologique et des ressources minérales de la République Gabonaise à 1/1 000 000. DGMG-Ministère des Mines, du Pétrole, des Hydrocarbures, Libreville, 384 p.

[8] Affaton, P., Kalsbeek, F., Boudzoumou, F., Trompette, R., Thrane, K. and Frei, R. (2015) The Pan-African West Congo Belt in the Republic of Congo (Congo Brazza-

ville): Stratigraphy of the Mayombe and West Congo Supergroups Studied by Detrital Zircon Geochronology. *Precambrian Research*, **272**, 185-202. https://doi.org/10.1016/j.precamres.2015.10.020

[9] Nsungani, P.C. (2012) La chaîne panafricaine du Nord-Ouest de l'Angola: Etude pétrostructurale, géochimique et géochronologique. Implications géodynamiques. Thèse, Université Montpellier II, Montpellier, 328 p.

[10] Hossié, G. (1980) Contribution à l'étude structurale de la chaîne Ouest-congolienne Pan-Africaine dans le Mayombe congolais. Thèse 3ème cycle, Université de Montpellier, 124 p.

[11] Fullgraf, T., Callec, Y., Thiéblemont, D., Gloaguen, E., Charles, N., Le Métour, J., Prian, J.-P., Boudzoumou, F., Delhaye-Prat, V., Moreau, F., Kebi-Tsoumou, S. and Ndiele, B. (2015) Notice explicative de la carte géologique de la République du Congo à 1/200 000, Feuille Dolisie. Éditions BRGM, 342 p.

[12] Bouénitéla, V. T. T. (2019) Le Domaine Paléoprotérozoïque (Eburnéen) de la Chaîne du Mayombe (Congo-Brazzaville): Origine et évolution tectono-métamorphique. Thèse, Université de Rennes1, Géosciences, Rennes, 448 p.

[13] Pemba-Boni, J. and Vellutini, P.J. (1991) Caractérisation géochimique des dykes basiques du massif de Les Saras (Mayombe Congolais, Afrique Centrale): Conséquences géodynamiques. *Journal of African Earth Sciences*, **14**, 209-215. https://doi.org/10.1016/0899-5362(92)90098-W

[14] Djama, L.M.J., Matiaba Bazika, U.V., Boudzoumou, F. and Mouzeo, K. (2018) Petrology and Geodynamic Context of Metabasic Rocks of Nemba Complex in the West Congo Fold Belt (Republic of Congo). *International Journal of Geosciences*, **9**, 1-18. https://doi.org/10.4236/ijg.2018.91001

[15] Vellutini, P., Rocci, G., Vicat, J.-P. and Gioan, P. (1983) Mise en évidence de complexes ophiolitiques dans la chaîne du Mayombe (Gabon-Angola) et nouvelle interprétation géotectonique. *Precambrian Research*, **22**, 1-21. https://doi.org/10.1016/0301-9268(83)90056-6

[16] Djama, L.M., Leterrier, J. and Michard, A. (1992) Pb, Sr and Nd Isotope Study of the Basement of the Mayumbian Belt (*Guena gneisses* and *Mfoubou granite*, Congo): Implications for Crustal Evolution in Central Africa. *Journal of African Earth Sciences*, **14**, 227-237. https://doi.org/10.1016/0899-5362(92)90100-Q

[17] Mpemba-Boni, J. (1990) Contribution à l'étude du magmatisme anté-pan africain de la chaîne du Mayombe. L'exemple du Massif de Les Saras (SW du Congo, Afrique Centrale) Pétrologie structurale-Géochimie-Géochronologie. Thèse, Université de Nancy 1, Nancy, 351 p.

[18] Dussin, I.A. and Dussin, T.M. (1995) Supergrupo Espinhaco: Modelo de evolucao geodinamica. *Geonomos*, **3**, 19-26. https://doi.org/10.18285/geonomos.v3i1.212

[19] Uhlein, A., Trompette, R. and Egydio-Silva, M. (1998) Proterozoic Rifting and Closure, SE Border of the São Francisco Craton, Brazil. *Journal of South American Earth Sciences*, **11**, 191-203. https://doi.org/10.1016/S0895-9811(98)00010-8

[20] Martins-Neto, M.A. (2000) Tectonics and Sedimentation in a Paleo/Mesopro- terozoic Rift-Sag Basin (Espinhaço Basin, Southeastern Brazil). *Precambrian Research*, **103**, 147-173. https://doi.org/10.1016/S0301-9268(00)00080-2

[21] Brito Neves, B.B.D., Winge, M. and Carneiro, M.A. (1996) Orogêneses precedendo e tafrogêneses sucedendo Rodinia na América do Sul. *Boletim IG-USP. Série Científica*, **27**, 1-40. https://doi.org/10.11606/issn.2316-8986.v27i0p1-40

[22] Cosson, J. (1955) Notice explicative sur les feuilles de Pointe-Noire et de Brazzaville.

Carte géologique de reconnaissance au 1/500,000e. Bulletin de la Direction des Mines et de la Géologie de l'Afrique Equatoriale Française, 56 p.

[23] Delpondor, F., Kant, F., Tack, L. and Préat, A. (2019) Cyclicity and Sequence Stratigraphy of the Neoproterozoic Uppermost Haut Shiloango-Lukala Carbonate Ramp System in the Lower Congo Region (Democratic Republic of the Congo): Example of Tectonostratigraphic Control versus Climatic Changes. *Journal of African Earth Sciences*, **160**, Article ID: 103636. https://doi.org/10.1016/j.jafrearsci.2019.103636

[24] Mickala, O.R., Vidal, L., Boudzoumou, F., Affaton, P., Vandamme, D., Borschneck, D. and Miche, H. (2014) Geochemical Characterization of the Marinoan "Cap Carbonate" of the Niari-Nyanga Basin (Central Africa). *Precambrian Research*, **255**, 367-380. https://doi.org/10.1016/j.precamres.2014.10.001

[25] Trompette, R. and Boudzoumou, F. (1988) Palaeogeographic Significance of Stromatolitic Buildups on Late Proterozoic Platforms: The Example of the West Congo Basin. *Palaeogeography*, *Palaeoclimatology*, *Palaeoecology*, **66**, 101-112. https://doi.org/10.1016/0031-0182(88)90083-1

[26] Préat, A., Delpondor, F., Ackouala Mfere, A.P. and Callec, Y. (2018) Paleoenvironments, δ13C and δ18O Signatures in the Neoproterozoic Carbonates of the Comba Basin, Republic of Congo: Implications for Regional Correlations and Marinoan Event. *Journal of African Earth Sciences*, **137**, 69-90. https://doi.org/10.1016/j.jafrearsci.2017.09.002

[27] Ackouala, A.P.M., Delpomdor, F., Proust, J.N., Boudzoumou, F., Callec, Y. and Préat, A. (2020) Facies and Architecture of the SCIc Formation (Schisto-Calcaire Group), Republic of the Congo, in the Niari-Nyanga and Comba Subbasins of the Neoproterozoic West Congo Basin after the Marinoan Glaciation Event. *Journal of African Earth Sciences*, **166**, Article ID: 103776. https://doi.org/10.1016/j.jafrearsci.2020.103776

[28] Pedrosa-Soares, A.C., Cordani, U.G. and Nutman, A. (2000) Constraining the Age of Neoproterozoic Glaciation in Eastern Brazil: First U-Pb (SHRIMP) Data of Detrital Zircons. *Revista Brasileira de Geociências*, **30**, 58-61. https://doi.org/10.25249/0375-7536.2000301058061

[29] Uhlein, A., Trompette, R. and Alvarenga, C.J. (1999) Neoproterozoic Glacial and Gravitational Sedimentation on a Continental Rifted Margin: The Jequitaı-Macaúbas Sequence (Minas Gerais, Brazil). *Journal of South American Earth Sciences*, **12**, 435-451. https://doi.org/10.1016/S0895-9811(99)00032-2

[30] Pedrosa-Soares, A.C., Noce, C.M., Wiedemann, C.M. and Pinto, C.P. (2001) The Araçuaı-West-Congo Orogen in Brazil: An Overview of a Confined Orogen Formed during Gondwanaland Assembly. *Precambrian Research*, **110**, 307-323. https://doi.org/10.1016/S0301-9268(01)00174-7

[31] Martins-Neto, M.A., Pedrosa-Soares, A.C. and Lima, S.A.A. (2001) Tecto-no-Sedimentary Evolution of Sedimentary Basins from Late Paleoproterozoic to Late Neoproterozoic in the Sao Francisco Craton and Araçuaı Fold Belt, Eastern Brazil. *Sedimentary Geology*, **141**, 343-370. https://doi.org/10.1016/S0037-0738(01)00082-3

[32] Pedrosa-Soares, A.C., Vidal, P., Leonardos, O.H. and Brito Neves, B.B.D. (1998) Neoproterozoic Oceanic Remnants in Eastern Brazil: Further Evidence and Refutation of an Exclusively Ensialic Evolution for the Araçuaí-West Congo Orogen. *Geology*, **26**, 519-522. https://doi.org/10.1130/0091-7613(1998)026<0519:NORIEB>2.3.CO;2

[33] Le Bayon, B., Callec, Y., Fullgraf, T., Lasseur, E., Thiéblemont, D., Charles, N.,

Gloaguen, E., Paquet, F., Gouin, J., Giresse, P., Makolobongo, B., Obambi, U., Moulounda Niangui, E. and Miassouka Mpika, R. (2015) Notice explicative de la carte géologique de la République du Congo à 1/200 000, feuille Conkouati. Editions BRGM, 242 p.

[34] Edgard, A.D. (1996) Kalsilite-Bearing Volcanics (Kamafugites). In: Mitchell, R.H., Ed., *Undersaturated Alkaline Rocks*: *Mineralogy*, *Petrologenesis*, *and Economic Potential*, Short Course Series 24, Mineralogical Association of Canada, Québec, 153-174.

[35] Bellieni, G., Comin-Chiaramonti, P., Marques, L.S., Melfi, A.J., Piccirillo, E.M., Nardy, A.J.R. and Roisenberg, A. (1984) Basaltes d'inondation à haute et basse teneur en TiO_2 du plateau du Paraná (Brésil): Aspects pétrologiques et géochimiques portant sur leur origine mantellique. *Neues Jahrbuch für Mineralogie Abhandlungen*, **150**, 273-306.

[36] Piccirillo, E.M., Comin-Chiaramonti, P., Melfi, A.J., Stolfa, D., Bellieni, G., Marques, L.S., Giaretta, A., Nardy, A.J.R., Pinese, J.P.P., Raposo, M.I.B. and Roisenberg, A. (1988) Petrochemistry of Continental Flood Basalt-Rhyolite Suites and Related Intrusives from the Parana Basin (Brazil). In: Piccirillo, E.M. and Melfi, A.J., Eds., *The Mesozoic Flood Volcanism of the Paraná Basin*: *Petrogenetic and Geophysical Aspects*, Instituto Astronomica e Geofisico Publishers, IAG-USP Press, São Paulo, 107-156. https://doi.org/10.1007/978-94-015-7805-9_6

[37] Peate, D.W., Mantovani, M.S. and Hawkesworth, C.J. (1988) Geochemical Stratigraphy of the Paraná Continental Flood Basalts: Borehole Evidence. *Revista Brasileira de Geociências*, **18**, 212-221. https://doi.org/10.25249/0375-7536.1988182212221

[38] Winchester, J.A. and Floyd, P.A. (1977) Geochemical Discrimination of Different Magma Series and Their Differentiation Products Using Immobile Elements. *Chemical Geology*, **20**, 325-343. https://doi.org/10.1016/0009-2541(77)90057-2

[39] Pearce, J.A. (1996) Sources and Settings of Granitic Rocks. *Episodes Journal of International Geoscience*, **19**, 120-125. https://doi.org/10.18814/epiiugs/1996/v19i4/005

[40] Nakamura, N. (1974) Determination of REE, Ba, Fe, Mg, Na and K in Carbonaceous and Ordinary Chondrites. *Geochimica et Cosmochimica Acta*, **38**, 757-775. https://doi.org/10.1016/0016-7037(74)90149-5

[41] Sun, S.S. and McDonough, W.F. (1989) Chemical and Isotopic Systematics of Oceanic Basalts: Implications for Mantle Composition and Processes. *Geological Society*, *London*, *Special Publications*, **42**, 313-345. https://doi.org/10.1144/GSL.SP.1989.042.01.19

[42] McDonough, W.F. and Sun, S.S. (1995) The Composition of the Earth. *Chemical Geology*, **120**, 223-253. https://doi.org/10.1016/0009-2541(94)00140-4

[43] Pearce, J.A. and Norry, M.J. (1979) Petrogenetic Implications of Ti, Zr, Y, and Nb Variations in Volcanic Rocks. *Contributions to Mineralogy and Petrology*, **69**, 33-47. https://doi.org/10.1007/BF00375192

[44] Pearce, J.A. (1983) Role of the Sub-Continental Lithosphere in Magma Genesis at Active Continental Margins. In: Hawkesworth, C.J. and Norry, M.J., Eds., *Continental Basalts and Mantle Xenoliths*, Shiva, Cheshire, 230-249.

[45] Wood, D.A. (1980) The Application of a Th-Hf-Ta Diagram to Problems of Tectonomagmatic Classification and to Establishing the Nature of Crustal Contamination of Basaltic Lavas of the British Tertiary Volcanic Province. *Earth and Planetary*

Science Letters, **50**, 11-30. https://doi.org/10.1016/0012-821X(80)90116-8

[46] Meschede, M. (1986) A Method of Discriminating between Different Types of Mid-Ocean Ridge Basalts and Continental Tholeiites with the Nb-1bZr-1bY Diagram. *Chemical Geology*, **56**, 207-218. https://doi.org/10.1016/0009-2541(86)90004-5

[47] Cabanis, P.B. and Thiéblemont, D. (1988) La discrimination des tholéiites continentales et des basaltes arrière-arc. Proposition d'un nouveau diagramme, le triangle Th-3Tb-2Ta. *Bulletin de la Société Géologique de France*, **4**, 927-935. https://doi.org/10.2113/gssgfbull.IV.6.927

[48] Thiéblemont, D., Chèvremont, P., Castaing, C., Triboulet, C. and Feybesse, J.L. (1994) La discrimination géotectonique des roches magmatiques basiques par les éléments traces. Réévaluation d'après une base de données et application à la chaîne panafricaine du Togo. *Geodinamica Acta*, **7**, 139-157. https://doi.org/10.1080/09853111.1994.11105264

[49] Luigi, B., Gianluca, B., Claudio, N. and Franca, S. (2009) Continental Flood Basalts and Mantle Plumes; a Case Study of the Northern Ethiopian. *Journal of Petrology*, **50**, 1377-1403. https://doi.org/10.1093/petrology/egp024

[50] Beard, C.D., Scoates, J.S., Weis, D., Bedard, H.J. and Dell'Oro, T.A. (2017) Geochemistry and Origin of the Neoproterozoic Natkusiak Flood Basalts and Related Franklin Sills, Victoria Island, Arctic Canada. *Journal of Petrology*, **58**, 2191-2220. https://doi.org/10.1093/petrology/egy004

[51] Xia, L. and Li, X. (2018) Basalt Geochemistry as a Diagnostic Indicator of Tectonic Setting. *Gondwana Research*, **65**, 43-67. https://doi.org/10.1016/j.gr.2018.08.006

[52] Cavalcante, C., Fossen, H., Almeida, R.P.D., Hollanda, M.H.B.M. and Egydio-Silva, M. (2019) Reviewing the Puzzling Intracontinental Termination of the Araçuaí-West Congo Orogenic Belt and Its Implications for Orogenic Development. *Precambrian Research*, **322**, 85-98. https://doi.org/10.1016/j.precamres.2018.12.025

[53] Alkmim, F.F., Marshak, S., Pedrosa-Soares, A.C., Peres, G.G., Cruz, S.C.P. and Whittington, A. (2006) Kinematic Evolution of the Araçuaí-West Congo Orogen in Brazil and Africa: Nutcracker Tectonics during the Neoproterozoic Assembly of Gondwana. *Precambrian Research*, **149**, 43-64. https://doi.org/10.1016/j.precamres.2006.06.007

[54] Richter, F., Lana, C., Stevens, G., Buick, I.S., Pedrosa-Soares, A.C., Alkmim, F.F. and Cuts, K. (2016) Sedimentation, Metamorphism and Granite Generation in a Back-Arc Region: Records from the Ediacaran Nova Vénécia Complex (Araçuaï Orogen): Southeastern Brazil. *Precambrian Research*, **272**, 78-100. https://doi.org/10.1016/j.precamres.2015.10.012

[55] Pearce, J.A. (2008) Geochemical Fingerprinting of Oceanic Basalts with Applications to Ophiolite Classification and the Search for Archean Oceanic Crust. *Lithos*, **100**, 14-48. https://doi.org/10.1016/j.lithos.2007.06.016

[56] Fitton, J.G., Saunders, A.D., Norry, M.J., Hardarson, B.S. and Taylor, R.N. (1997) Thermal and Chemical Structure of the Iceland Plume. *Earth and Planetary Science Letters*, **153**, 197-208. https://doi.org/10.1016/S0012-821X(97)00170-2

[57] Condie, K.C. (2003) Incompatible Element Ratios in Oceanic Basalts and Komatiites: Tracking Deep Mantle Sources and Continental Growth Rates with Time. *Geochemistry, Geophysics, Geosystems*, **4**, 1-28. https://doi.org/10.1029/2002GC000333

[58] Condie, K.C. (2005) High Field Strength Element Ratios in Archean Basalts: A Window to Evolving Sources of Mantle Plumes. *Lithos*, **79**, 491-504. https://doi.org/10.1016/j.lithos.2004.09.014